Immunity

Agonistic anti-CD40 antibody treatment converts resident regulatory T cells into activated type 1 effectors within the tumor microenvironment

Highlights

- Agonistic αCD40 reduced tumor Treg cells via loss of Foxp3 to generate "ExTreg" cells
- ExTreg cells required DCs and IL-12/IFN-γ and accumulated with DCs at the tumor border
- ExTreg cells acquired Tbet and *Ifng* expression aligned with anti-tumor effector T cells
- Nuclear NFAT1 revealed increased antigen reactivity among ExTreg cells after αCD40

Authors

Vivien I. Maltez, Charu Arora, Kyle P. Gribbin, ..., Robert H. Vonderheide, Ronald N. Germain, Katelyn T. Byrne

Correspondence

rgermain@niaid.nih.gov (R.N.G.), byrneka@ohsu.edu (K.T.B.)

In brief

Regulatory T (Treg) cells are phenotypically stable in inflammatory settings. Maltez et al. report that αCD40 immunotherapy induced conversion of Treg cells into FoxP3^{-}Tbet^{+}IFN-γ^{+} "ExTreg" cells within the tumor microenvironment. ExTreg cells exhibited increased antigen reactivity and spatially associated with Cxcl9^{+}dendritic cells in the tumor periphery, suggesting plasticity and anti-tumor potential.

Maltez et al., 2026, Immunity *59*, 1–17
April 14, 2026 © 2026 Elsevier Inc. All rights are reserved, including those for text and data mining, AI training, and similar technologies.
https://doi.org/10.1016/j.immuni.2026.03.011

CellPress

Please cite this article in press as: Maltez et al., Agonistic anti-CD40 antibody treatment converts resident regulatory T cells into activated type 1 effectors within the tumor microenvironment, Immunity (2026), https://doi.org/10.1016/j.immuni.2026.03.011

Immunity

CellPress

Article

Agonistic anti-CD40 antibody treatment converts resident regulatory T cells into activated type 1 effectors within the tumor microenvironment

Vivien I. Maltez,[1,2,12] Charu Arora,[3] Kyle P. Gribbin,[4] Breanna Caruso,[4] Margaret E. Haerr,[4,5] Rina Sor,[3] Qiaoshi Lian,[2] Katie E. Blise,[6,7] Shamilene Sivagnanam,[4,7] Rosalie C. Sears,[7,8,9] Lisa M. Coussens,[4,7] Robert H. Vonderheide,[3,10] Ronald N. Germain,[2,11,13,*] and Katelyn T. Byrne[4,7,9,10,13,14,*]

[1]Postdoctoral Research Associate Training (PRAT) Program Fellow, NIGMS, NIH, Bethesda, MD, USA
[2]Lymphocyte Biology Section, Laboratory of Immune System Biology, NIAID, NIH, Bethesda, MD, USA
[3]Abramson Cancer Center, Perelman School of Medicine, University of Pennsylvania, Philadelphia, PA, USA
[4]Department of Cell, Developmental and Cancer Biology, Oregon Health and Science University, Portland, OR, USA
[5]Graduate Program in Biomedical Sciences, Oregon Health and Science University, Portland, OR, USA
[6]Department of Biomedical Engineering, Oregon Health and Science University, Portland, OR, USA
[7]The Knight Cancer Institute, Oregon Health and Science University, Portland, OR, USA
[8]Department of Molecular and Medical Genetics, Oregon Health and Science University, Portland, OR, USA
[9]Brenden-Colson Center for Pancreatic Care, Oregon Health and Science University, Portland, OR, USA
[10]Parker Institute for Cancer Immunotherapy, University of Pennsylvania, Philadelphia, PA, USA
[11]Center for Advanced Tissue Imaging (CAT-I), NIAID and NCI, NIH, Bethesda, MD, USA
[12]Present address: Division of Allergy, Immunology and Rheumatology, Department of Pediatrics, University of California, San Diego, San Diego, CA, USA
[13]These authors contributed equally
[14]Lead contact
*Correspondence: rgermain@niaid.nih.gov (R.N.G.), byrneka@ohsu.edu (K.T.B.)
https://doi.org/10.1016/j.immuni.2026.03.011

SUMMARY

In pancreatic ductal adenocarcinoma (PDAC), agonistic anti-CD40 (αCD40) reduces frequencies of intratumoral regulatory T (Treg) cells despite a lack of CD40 expression on Treg cells. Here, we leveraged spatiotemporal imaging and lineage tracing approaches to examine intratumoral Treg cell fate in a mouse model of PDAC, where immune checkpoint blockade (ICB) (αPD-1 + αCTLA-4) combined with αCD40 controls tumor growth. Intratumoral Foxp3$^+$ Treg cell numbers collapsed upon treatment, dependent on CD40-activated dendritic cells (DCs) and induction of interleukin (IL)-12 and interferon (IFN)-γ. This reduction corresponded with cellular alterations; Treg cells acquired an "ExTreg" phenotype characterized by loss of Foxp3 expression and acquisition of T helper 1 (Th1)-like features (Tbet$^+$IFN-γ^+). αCD40 promoted a spatially reorganized tumor microenvironment (TME), with *Cxcr3*$^+$ Treg and ExTreg cells localized to the tumor periphery with *Cxcl9*-expressing DCs. Through *in situ* analyses of T cell receptor (TCR) signaling, we found that ExTreg cells had the highest antigen-driven activation among tumor-infiltrating T cells. Reprogramming of intratumoral Treg cells into Th1-like effectors reveals plasticity and an anti-tumor capacity of these cells.

INTRODUCTION

Cancer cells drive feedforward suppressive programming within the tumor microenvironment (TME),[1] which is a barrier to anti-tumor immunity. Surmounting these obstacles is sometimes possible through immune checkpoint blockade (ICB) for certain tumor types. Antibody-mediated blockade of programmed death-1 (PD-1) (αPD-1) expands active effector T (T eff) cells from stem-like progenitors[2] and overcomes inhibition of T cell receptor (TCR) signaling[3,4] to enable anti-tumor activity. Antibodies targeting cytotoxic T lymphocyte associated protein-4 (CTLA-4) (αCTLA-4) preserve costimulatory signals,[5] and in some models, they deplete immunosuppressive regulatory Foxp3$^+$CD4$^+$ T (Treg) cells via antibody-dependent cellular cytotoxicity (ADCC).[6] However, ICB therapy fails in many clinical settings,[7] requiring additional TME perturbations.

To promote immunotherapy sensitivity in the TME, we have employed agonistic anti-CD40 (αCD40). CD40 stimulation promotes the maturation of antigen-presenting cells (APCs) and dendritic cells (DCs), driving the stimulation and activation of T eff cells[8–10] that promote tumor rejection. In *Kras^{G12D}Trp53^{R172H}Pdx-1-Cre* YFP (KPCY) mouse models of pancreatic ductal adenocarcinoma (PDAC),[11] αCD40 induces T cell-mediated tumor rejection via increased production of type 1 cytokines,[12,13] a feature recapitulated in clinical data from patients receiving αCD40 therapy.[14–16] Agonistic αCD40

All rights are reserved, including those for text and data mining, AI training, and similar technologies.

Please cite this article in press as: Maltez et al., Agonistic anti-CD40 antibody treatment converts resident regulatory T cells into activated type 1 effectors within the tumor microenvironment, Immunity (2026), https://doi.org/10.1016/j.immuni.2026.03.011

increased survival in a successful phase II trial for patients with metastatic PDAC[17] and showed systemic tumor regressions in patients with ICB-resistant tumors,[18] although not all trials and cohorts showed such positive outcomes.[16] Thus, while αCD40 therapies may promote clinically useful immune responses in many tumor types, optimizing use of this modality requires more detailed information on the effects of such treatment within tumors and lymphoid tissues.

Agonistic αCD40 not only enhances APC function in the TME[12,19] but also reduces Treg cells.[12,13] Treg cells use multiple mechanisms to limit anti-tumor immunity, including sequestering interleukin (IL)-2,[20] preventing costimulation,[21] and forming suppressive metabolites.[22,23] Given the substantial effort to target tumor-associated Treg cells[24] via elimination,[25,26] functional blockade,[5,27–29] migration prevention,[30,31] or altered cytokine production,[32–35] determining how αCD40 reduces the number of intratumoral Treg cells is warranted—with the effect likely indirect, as this molecule is not commonly expressed by Treg cells.[36]

Here, we leveraged a spatiotemporal approach to evaluate intratumoral Treg cell fate after αCD40 ± ICB. Intratumoral Treg cell numbers collapsed in a manner dependent on CD40-activated DCs and induction of IL-12 and interferon (IFN)-γ. The reduction in Treg cell numbers corresponded with cellular alterations; Treg cells acquired an "ExTreg" phenotype characterized by a loss of Foxp3 and acquisition of T helper 1 (Th1)-like features, including expression of Tbet and IFN-γ. *Cxcl9* production by DCs and DC-adjacent cells was associated with recruitment of *Cxcr3*$^+$ Treg and ExTreg cells to the tumor edge. Thus, αCD40-induced type 1 inflammation altered functional Treg cell fate concomitant with a marked spatial reorganization of DCs and Treg cells within the TME. These findings show that intratumoral Treg cells—a normally stable CD4$^+$ T cell subset[37]—are efficiently converted into Th1-like effector cells after agonistic αCD40, suggesting that a poor prognostic tissue state (Treg cell-rich TME) could, through suitable intervention, improve anti-tumor responses.

RESULTS

Agonistic αCD40 stimulation drives loss of intratumoral Treg cells

Mice bearing a subcutaneously implanted clonal derivative of a genetically induced KPCY (T cell high) tumor[11] were treated with three doses of dual ICB (αPD-1 and αCTLA-4, "PC"), a single dose of αCD40 (clone FGK4.5, "F"), or both ICB and αCD40 ("FPC"), resulting in tumor control as reported[13] (Figures S1A and S1B). We examined intratumoral Treg cells 10 days after FPC, employing multiplex tissue imaging[38] to evaluate the spatial aspects of Treg cell loss without the confounding effects of differential extraction of T cells. As early as 48 h after αCD40 in FPC-treated mice, there was a substantial reduction in Treg cells vs. isotype control-treated mice (Figures 1A and 1B). The *in situ* Treg cell loss agreed with flow cytometry of extracted cells (Figures 1C and S1C) and was not observed in non-Treg cell subsets (Figure 1D). Treg cells were also reduced in polyclonal 4,662 KPC tumors (as we have previous reported[12,13]), B16 melanoma, and MC38 colorectal and orthotopically implanted KPC tumors after treatment (Figures S1D–S1F), showing that αCD40 rapidly impacted Treg cell fate in multiple TMEs. The remaining Treg cells localized preferentially near the tumor periphery, while other T eff cells are distributed more homogenously in the TME (Figure 1E).

Intratumoral Treg cell reduction occurs in some tumors due to αCTLA-4-mediated ADCC,[6] but this is not observed in the PDAC TME.[13] Nonetheless, we re-examined the contribution of each FPC component in Treg cell loss and redistribution in the TME. The numbers of intratumoral Treg cells were significantly reduced in mice given αCD40 alone or in combination with PC vs. control-treated animals (Figures 1F–1H), differing from prior Treg cellular plasticity studies.[39] Furthermore, Treg cells were predominantly located at the tumor edge only after αCD40 (Figure 1I). In contrast, αCTLA-4 alone or with αPD-1 did not reduce Treg cells (Figures 1G, 1H, and S1G), nor did it affect their spatial distribution (Figure 1I). Host expression of CD40 was required for therapy-induced Treg cell reduction, regardless of treatment with αCTLA-4 (Figures S1H–S1J), and Treg cell expression of CD40L was unchanged with αCD40 ± ICB (Figure S1K). Together, these data indicate that αCD40 impacted the intratumoral Treg cells independent of ICB.

Role of cDC1s and type 1 cytokines in mediating Foxp3$^+$ CD4$^+$ Treg cell loss in the TME

Treg cells do not normally express CD40,[36] including in the mouse PDAC TME (Figure S2A). In contrast, conventional type 1 DCs (cDC1s) are a major target of αCD40[19,40] and the dominant CD40$^+$ population in the PDAC TME (Figure S2A, cDC1: *Cd3*$^-$*Itgae*$^+$*Xcr1*$^+$).[38,41,42] cDC1s play a role in bridging innate and adaptive immune responses.[40] To examine if αCD40 acted to reduce Treg cells via cDC1, we used FPC treatment of tumor-bearing *Batf3*$^{-/-}$ mice.[43] In *Batf3*$^{-/-}$ mice, αCD40 failed to reduce or relocalize Treg cells (Figures 2A–2C and S2B–S2H).

CD40-matured DCs produce the type 1 cytokine, IL-12, which amplifies production of the anti-tumor cytokine IFN-γ,[44,45] and both cytokines were required for tumor control after FPC (Figures S2I and S2J). Intratumoral Foxp3$^+$ Treg cell frequencies were not reduced in *IL-12p40*$^{-/-}$[46] and *IFN-γ*$^{-/-}$[47] mice by αCD40, indicating that Treg cell loss required the action of these cytokines (Figures S2K and S2L). To exclude a confounding role of TME baseline alterations in these Th1-cytokine-deficient mice, we also examined tumors from wild-type (WT) mice treated with blocking antibodies targeting IL-12p40 or IFN-γ beginning 1 day before αCD40 administration. αCD40 Treg cell reduction and polarized localization were lost upon cytokine blockade (Figures 2D–2F). These data indicate that the IL-12/IFN-γ cytokine axis is critical to αCD40-induced intratumoral Treg cell loss.

Anti-CD40 treatment generates Foxp3$^-$ ExTreg cells

The rapid reduction of Treg cells in the PDAC TME of animals treated with αCD40 could reflect Treg cell-specific apoptosis, efflux of Treg cells to the tumor-draining lymph node (TdLN), or the abrogation of Foxp3 expression, with the latter predicting Treg cell loss without cell death. We examined the apoptotic marker cleaved caspase-3 (CC3) in Treg cells 48 h after αCD40 and found that the proportion of CC3$^+$ Treg cells was equivalent ± FPC (Figure S3A). Treg cell proportions were slightly increased within the TdLN 48 h after αCD40 (Figure S3B); however, this did not account for the cell loss in the TME, suggesting that loss of Foxp3 expression by intratumoral Treg cells may account for the reduction in the number of Foxp3$^+$CD4$^+$ T cells.

Please cite this article in press as: Maltez et al., Agonistic anti-CD40 antibody treatment converts resident regulatory T cells into activated type 1 effectors within the tumor microenvironment, Immunity (2026), https://doi.org/10.1016/j.immuni.2026.03.011

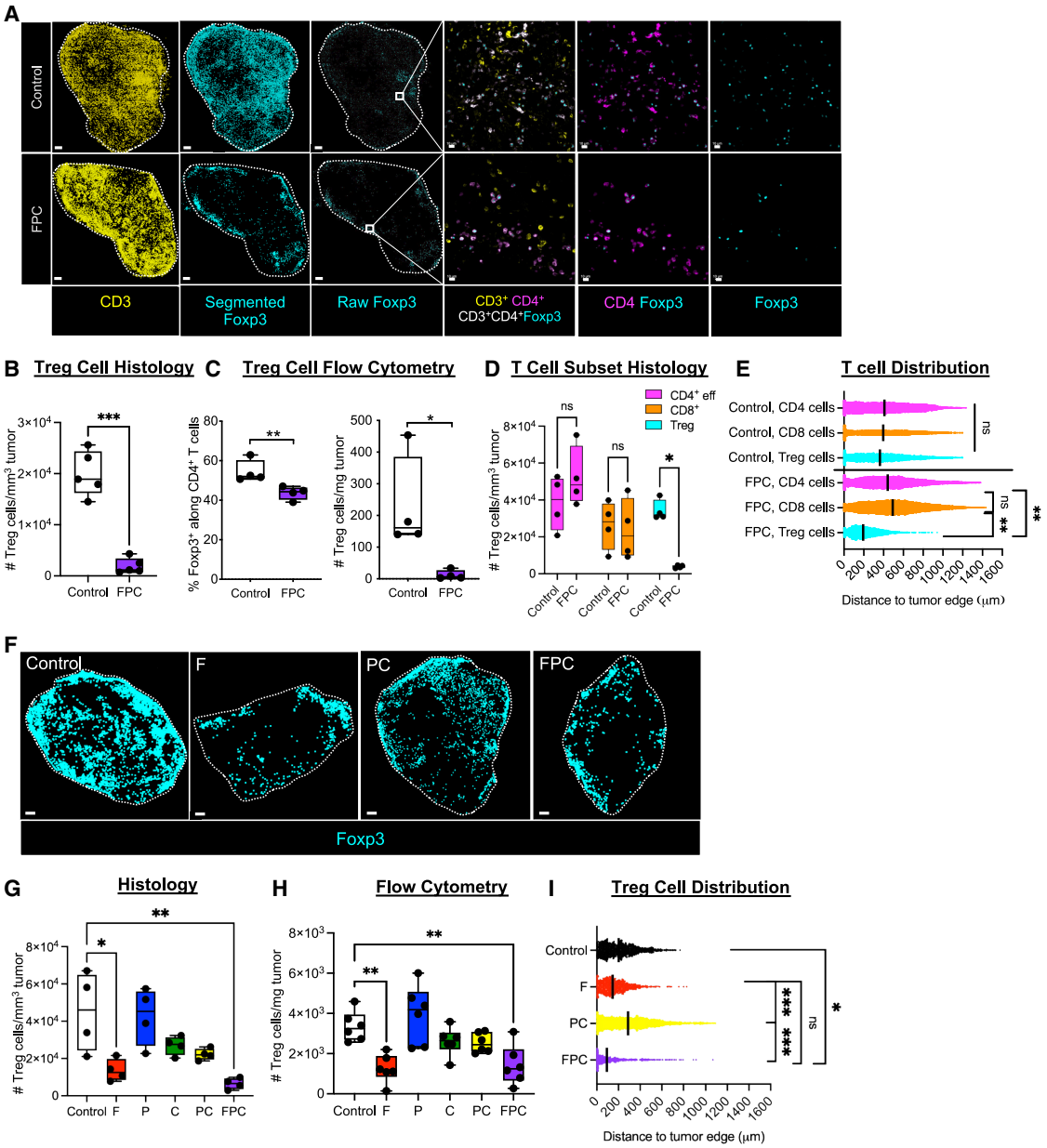

Figure 1. Agonistic CD40 therapy reduces intratumoral Treg cells independently of anti-CTLA-4 treatment

WT C57BL/6 mice were subcutaneously injected with KPCY T cell high tumor clone 2838c3. Mice were treated with anti-PD-1 (P) and anti-CTLA-4 (C) on days 12 and 15, with a single dose of agonistic anti-CD40 (F) on day 15 (as a single agent), or with a combination treatment (FPC). Tumors were harvested on day 17.

(A) Segmented images and raw marker expression.

(B and C) Treg cells were quantified by (B) IF or (C) flow cytometry among live, CD45$^+$ cells (left) and per mg of tumor (right).

(D and E) Total non-Treg CD4$^+$, CD8$^+$ T, and Treg cell distance to tumor edge.

(F–I) Indicated treatments with quantification IF (G), flow cytometry (H), or spatial distribution (I). Data represent 2–5 experiments with n = 4–7 mice/group; each symbol represents an individual mouse (B–D, G, and H) or cells (E and I). Boxplots: median + IQR, whiskers indicate range. (D) and (E), same experiment; (G) and (I), same experiment, with the indicated number of mice in (D) and (G), respectively. Scale bars: 200 μm (A and F), 10 μm for zoom insets (A). Dotted line: tumor edge (A and F). Stats: unpaired t test (B and C), one-way ANOVA with Tukey's post-test (D, G, and H), and mean difference calculations as appropriate (E and I). Significance: *p < 0.05, **p < 0.01, ***p < 0.001, ****p < 0.0001 (B–D, G, and H). Distance plots (E and I) ANOVA p < 0.0001, with mean difference of *p > 50 μm, **p > 100 μm, ***p > 150 μm, ****p > 200 μm.

Partial, although rarely complete, loss of Foxp3 by Treg cells has been described in settings of inflammation, including infections[48] and autoimmunity,[37] or vaccination with Toll-like receptor agonists.[49] To examine Foxp3 loss in the PDAC TME after αCD40, we conducted Foxp3 lineage tracing[50] using *Foxp3*$^{eGFP\text{-}Cre\text{-}ERT2}$ × *Gt(ROSA)26Sor*$^{tm(CAG\text{-}tdTomato)/Hze}$ (R26td Tomato) mice, where tamoxifen (TMX) administration permanently labels Foxp3-expressing cells by tdTomato expression,

Please cite this article in press as: Maltez et al., Agonistic anti-CD40 antibody treatment converts resident regulatory T cells into activated type 1 effectors within the tumor microenvironment, Immunity (2026), https://doi.org/10.1016/j.immuni.2026.03.011

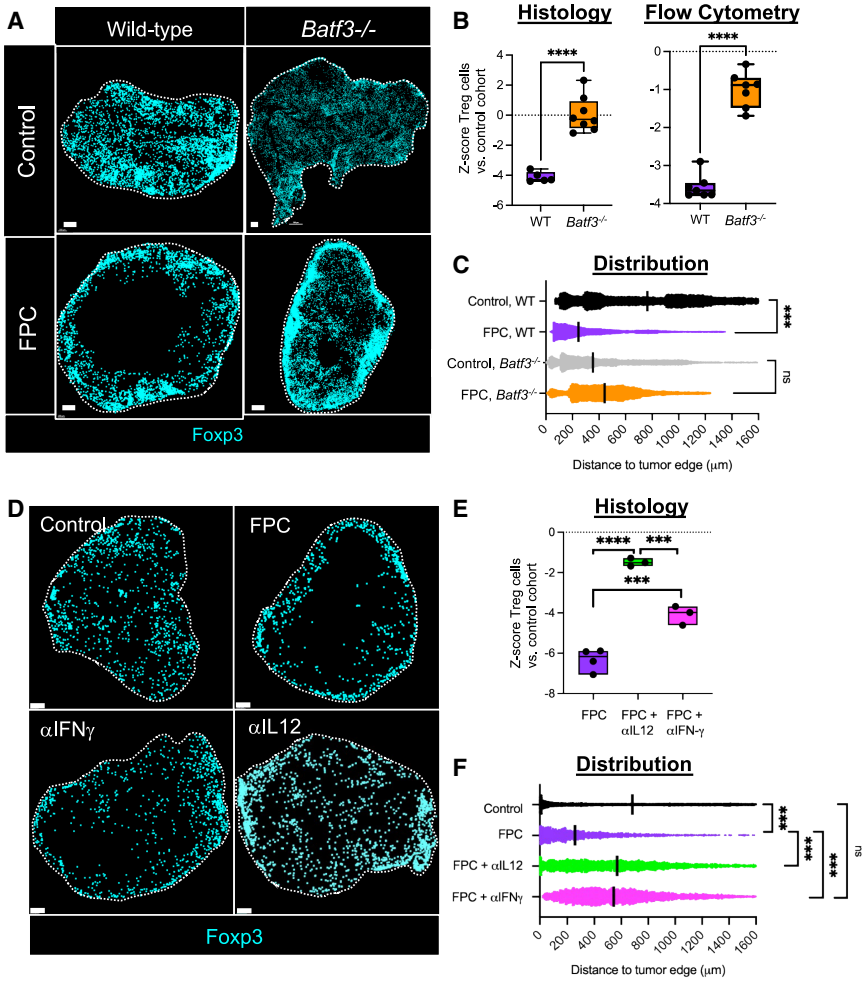

Figure 2. Anti-CD40 antibody-induced Treg cell loss is mediated by DCs and the IL-12/IFN-γ cytokine axis

(A–C) WT or *Batf3*$^{-/-}$ mice were treated as in Figure 1A. Segmented Treg cells shown in (A), quantified as standardized *Z* scores vs. control (B) and assessed for localization (C).

(D–F) Mice were treated ±IFN-γ or IL-12p40 blockade 2 days before therapy initiation. Treg cells shown in (D), quantified *Z* scores vs. control (E) and assessed for localization (F). Data represent 2–5 experiments with $n = 3$–8 mice per group; each symbol indicates a single mouse (B and E) or cell (C and F), whiskers indicate the range in (B). Boxplots: median + IQR. (B and C) From the same experiment, *n* in (B); (E and F) from the same experiment, with *n* in (E). Scale bars: 200 μm, and dotted line indicates tumor edge (A and D). Stats: unpaired *t* test (B), one-way ANOVA with Tukey's post-test (E), one-way ANOVA with Tukey's post-test and mean difference calculations when appropriate (C and F). Significance: $^{*}p < 0.05$, $^{**}p < 0.01$, $^{***}p < 0.001$, $^{****}p < 0.0001$. For distance to edge plots (C and F) ANOVA $p < 0.0001$, with mean difference of $^{*}p > 50$ μm, $^{**}p > 100$ μm, $^{***}p > 150$ μm, $^{****}p > 200$ μm.

while ongoing transcription at the Foxp3 locus is reported by GFP expression and/or direct Foxp3 protein staining. Tumors were implanted and established in Foxp3-lineage mice, at which point mice received TMX for 3 days to irreversibly label Foxp3-expressing Treg cells. Mice were rested for 2 days before initiating FPC, followed by harvesting and assessment of tumors 48 h after αCD40 (day 5 after the start of therapy). We identified conventional Treg cells (cTreg cells) as CD4^{+} T cells that immunostained for Foxp3 and expressed tdTomato (Foxp3^{+} Lineage^{+}), while ExTreg cells were identified as CD4^{+} T cells that retained tdTomato but lacked Foxp3 (Foxp3^{-}Lineage^{+}; Figure 3A). cTreg cells were significantly reduced in tumors after FPC (Figures 3A and 3B), although some CD25^{+} cTreg cells remained (Figure S3C). However, ExTreg cells were significantly increased in tumors of FPC-treated mice, as compared with those in tumors of control-treated mice (Figures 3A, 3B, and S3D). Treatment-induced ExTreg cell conversion was specific for the tumor site, as no increase in the proportion of ExTreg cells was observed in the TdLN, liver, or spleen 48 h after αCD40 (Figures S3E and S3F). The proportions of cTreg and ExTreg cells in the TME of treated mice were similar after FTY720 administration, a sphingosine-1 phosphate agonist that inhibits lymphocyte egress from lymph nodes[51] (Figure S3G), indicating that ExTreg cells arose locally in the tumor site. A trend toward increased ExTreg cells was also observed in MC38 or orthotopically implanted PDAC tumors 48 h after FPC (Figures S3H and S3I). Together, these data indicate that the change in intratumoral Treg cell number of FPC-treated mice was not a result of increased cTreg cell death or TME efflux. Instead, Treg cell reduction was due to a loss of Foxp3 expression among Treg cells in the context of αCD40. A time course examining the Foxp3-lineage-marked T cells after FPC treatment was consistent with these findings, revealing a dominance of ExTreg cells as early as 16 h after αCD40 and an increase over 2 days post-FPC (Figure 3C), concurrent with Foxp3-lineage T cell enrichment at the tumor edge (Figure 3D). Changes in Treg cell subsets were not transient, with no recovery of cTreg cells or further loss of ExTreg cells 10 days after αCD40 (Figure S3J).

Because αCD40 was specifically required for loss of Foxp3^{+}CD4^{+} T cells in this model, we assessed the development of ExTreg cells in PC- vs. FPC-treated mice. ExTreg cell induction (Figures 3E and 3F) and the spatial redistribution of Treg cells within the tumor occurred only in mice that received αCD40 (Figure 3G). These data parallel our observation that αCD40 drove Foxp3^{+} Treg cell loss and concurrent cellular reorganization.

Given that blockade of IL-12/IFN-γ disrupted intratumoral αCD40-induced changes in cTreg cells, we tested for a similar impact on the generation of ExTreg cells, including on the intratumoral *in situ* organization of cells.[38] Mice receiving FPC along with IL-12p40- or IFN-γ-blocking antibodies had fewer

Please cite this article in press as: Maltez et al., Agonistic anti-CD40 antibody treatment converts resident regulatory T cells into activated type 1 effectors within the tumor microenvironment, Immunity (2026), https://doi.org/10.1016/j.immuni.2026.03.011

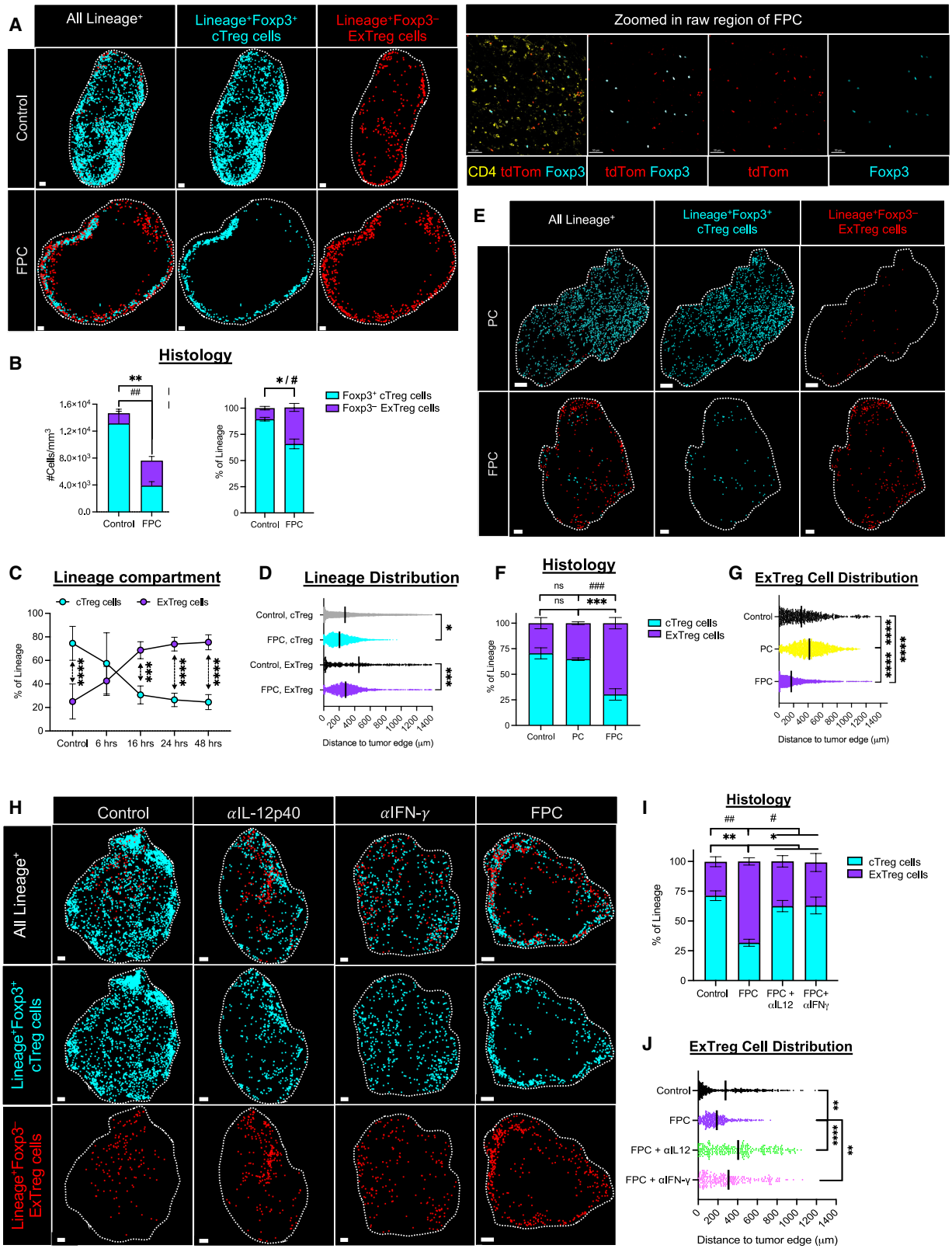

(legend on next page)

Please cite this article in press as: Maltez et al., Agonistic anti-CD40 antibody treatment converts resident regulatory T cells into activated type 1 effectors within the tumor microenvironment, Immunity (2026), https://doi.org/10.1016/j.immuni.2026.03.011

intratumoral ExTreg cells (Figures 3H and 3I) and lacked concentration of these cells at the tumor edge (Figure 3J). Type 1 inflammation in the gut alters Foxp3 expression by Treg cells,[48] consistent with our conclusion that induction of type 1 cytokines via αCD40 of DCs in the TME fosters Treg plasticity.

αCD40 induces Th1 transcription factor skewing in ExTreg cells

Treg cell-suppressive function (and Foxp3 itself) is stabilized by the supportive transcription factor, Helios,[52,53] which we used as a proxy for Treg cell phenotype preservation after αCD40. The percentage of Helios$^+$ cTreg cells dropped significantly after FPC, while ExTreg cells were predominantly Helios$^-$ regardless of treatment (Figures 4A and 4B). Helios is linked to centrally induced vs. peripherally induced Treg cells,[52] and we observed similar proportions of ExTreg cells in the PDAC TME 48 h after αCD40 whether Foxp3-lineage labeling occurred before or after tumor implantation (Figure S4A). These data support the conclusion that ExTreg cells are derived from preexisting cTreg cells, in agreement with a recent report from Dykema and colleagues.[54] Our data show ExTreg cell generation occurred in the TME, where T cells are inherently not naive, indicating that Foxp3-lineage-labeled cells do not represent T eff cells with transient expression of Foxp3.[39]

The role of IL-12 and IFN-γ in promoting Foxp3 expression loss led us to hypothesize that another transcription factor—specifically Tbet, the master transcription factor for Th1 eff cell responses[55]—was upregulated in ExTreg cells. Foxp3 and Tbet have diametrically opposed functions,[56] and previous studies indicate that Treg cells exposed to type 1 inflammation can gain Th1 cell effector functions,[39] often dependent on Tbet. We first examined phosphorylated STAT1 (pSTAT1), indicative of IFN signaling,[57] in the TME of FPC-treated animals. The proportion of ExTreg cells that expressed pSTAT1 was greatly increased in the TME of αCD40-treated but not control- or PC-treated mice (Figures 4C and S4B, top). This contrasts with the fraction of Treg cells that expressed pSTAT5 (indicative of IL-2 signaling[58]), which was significantly decreased in tumors of FPC-treated mice as compared with those from control- and PC-treated mice (Figures S4B bottom and S4C). Additionally, pSTAT1 signaling was lost in FPC-treated TMEs after IL-12 or IFN-γ blockade (Figures S4D and S4E). Consistent with prior data showing that IFN-γ, but not the type 1 IFN receptor (IFNAR), is required for FPC efficacy,[13] these data support IFN-γ as a major driver of pSTAT1 signaling in ExTreg cells after αCD40.

Tbet is upregulated downstream of pSTAT1 signaling, typically due to IFN signaling,[57] and drives IL-12 receptor expression[59] and IFN-γ production in CD4$^+$ T cells.[60] To directly assess Tbet expression among Treg cells after αCD40, we examined Tbet$^+$Foxp3$^+$CD4$^+$ T cells in WT PDAC-bearing mice with or without FPC. There was a modest increase in the proportion of Tbet$^+$ cTreg cells after FPC treatment; this was not accompanied by a change in the expression of TCF1 and Blimp1, linked to Treg-suppressive functions (Figures S4F–S4H).[61,62] This finding was confirmed using Tbet/Foxp3 dual fluorescent reporter mice, revealing that in the context of FPC, Foxp3$^+$CD4$^+$ T cells increased expression of Tbet (Figures 4D and 4E). Using Foxp3-lineage mice to identify both cTreg and ExTreg cells, we found that FPC resulted in an increased frequency of Tbet$^+$Foxp3-lineage subsets vs. control treatment (Figures 4F and S4I). Tbet upregulation by both Foxp3-lineage subsets is consistent with prior studies linking Tbet gain to partial or even full Foxp3 loss in type 1 inflammatory conditions.[48]

ExTreg cells produce IFN-γ *in situ*, dependent on IL-12 and IFN-γ signaling

As Foxp3 is critical to the suppressive activity of Treg cells, αCD40-induced loss of Foxp3 expression may limit immune-inhibitory effects of Treg cells in the TME. But does type 1 inflammation also endow intratumoral Treg cells with distinct effector functions? Our observation of increased Tbet expression in Foxp3-lineage cells after αCD40 suggested that Treg cells could acquire Th1 eff cell functions. Tbet is expressed by *bona fide* suppressive cTreg cells,[48,63,64] but the functional activity of Tbet$^+$ ExTreg cells lacking Foxp3 was unclear, as complete Foxp3 loss vs. transcriptional competition could yield distinct phenotypes.[65]

To examine the functional phenotype of ExTreg cells *in situ*, we used RNAscope to detect *Ifng* transcripts, as IFN-γ is a Tbet-regulated cytokine with a well-established role in anti-tumor immunity.[66] Both the proportion and absolute numbers of *Ifng*$^+$ ExTreg cells *in situ* were significantly increased in the TME of FPC-treated mice as compared with control-treated mice (Figures 4G, 4H, and S4J, right). Notably, the number of *Ifng*$^+$ ExTreg cells was comparable to that of the entire non-Treg CD3$^+$

Figure 3. CD40-driven Treg cell conversion to ExTreg cells is regulated by the IL-12/IFN-γ axis

Tamoxifen-inducible Foxp3-lineage tracing mice were used for all experiments described. Foxp3-lineage mice received tamoxifen on days 8–10 post-tumor implantation, followed by indicated treatments. Tumors were analyzed for the endogenous lineage tracing marker (tdTomato) and for Foxp3 (by antibody staining).

(A and B) CD3$^+$/CD4$^+$ Lineage$^+$Foxp3$^+$ cTreg and Lineage$^+$Foxp3$^-$ ExTreg cells, shown via segmented data (left) and raw markers (right), were quantified for cell number and proportion as shown in (B).

(C and D) (C) Percentage of cTreg and ExTreg cells within the Foxp3-lineage compartment over time post-FPC and (D) distance to tumor edge.

(E–G) Foxp3-lineage mice treated with PC ± F (E), with proportions of cTreg or ExTreg cells (F) and distribution of ExTreg cells (G).

(H–J) Mice were treated ± FPC or FPC + IL-12p40/IFN-γ-blocking antibodies beginning 2 days before FPC. Tumors were analyzed for cTreg cells (H), ExTreg cells (I), and ExTreg cell distribution (J). Data represent 2–5 experiments with n = 3–5 mice/group; each symbol represents the value of the indicated group with error bars indicating the SD (B, F, and I), or an individual cell (D, G, and J). Panel numbers: (B and D) 5; (C, F, I, and J) 4; (G) 3. Scale bars: 200 μm for all but (A) zoom (50 μm); dotted line indicates tumor edge (A, E, and H). Stats: two-way ANOVA (C), one-way ANOVA (B), both with Tukey's post-test, or one-way ANOVA with Tukey's post-test and mean difference calculations when appropriate (D, G, and J). Significance: *$p < 0.05$, **$p < 0.01$, ***$p < 0.001$, ****$p < 0.0001$. All symbols use the same scaling as described for p values with (*). For distance to edge plots (D, G, and J) ANOVA $p < 0.0001$, with mean difference of *$p > 50$ μm, **$p > 100$ μm, ***$p > 150$ μm, ****$p > 200$ μm.

Please cite this article in press as: Maltez et al., Agonistic anti-CD40 antibody treatment converts resident regulatory T cells into activated type 1 effectors within the tumor microenvironment, Immunity (2026), https://doi.org/10.1016/j.immuni.2026.03.011

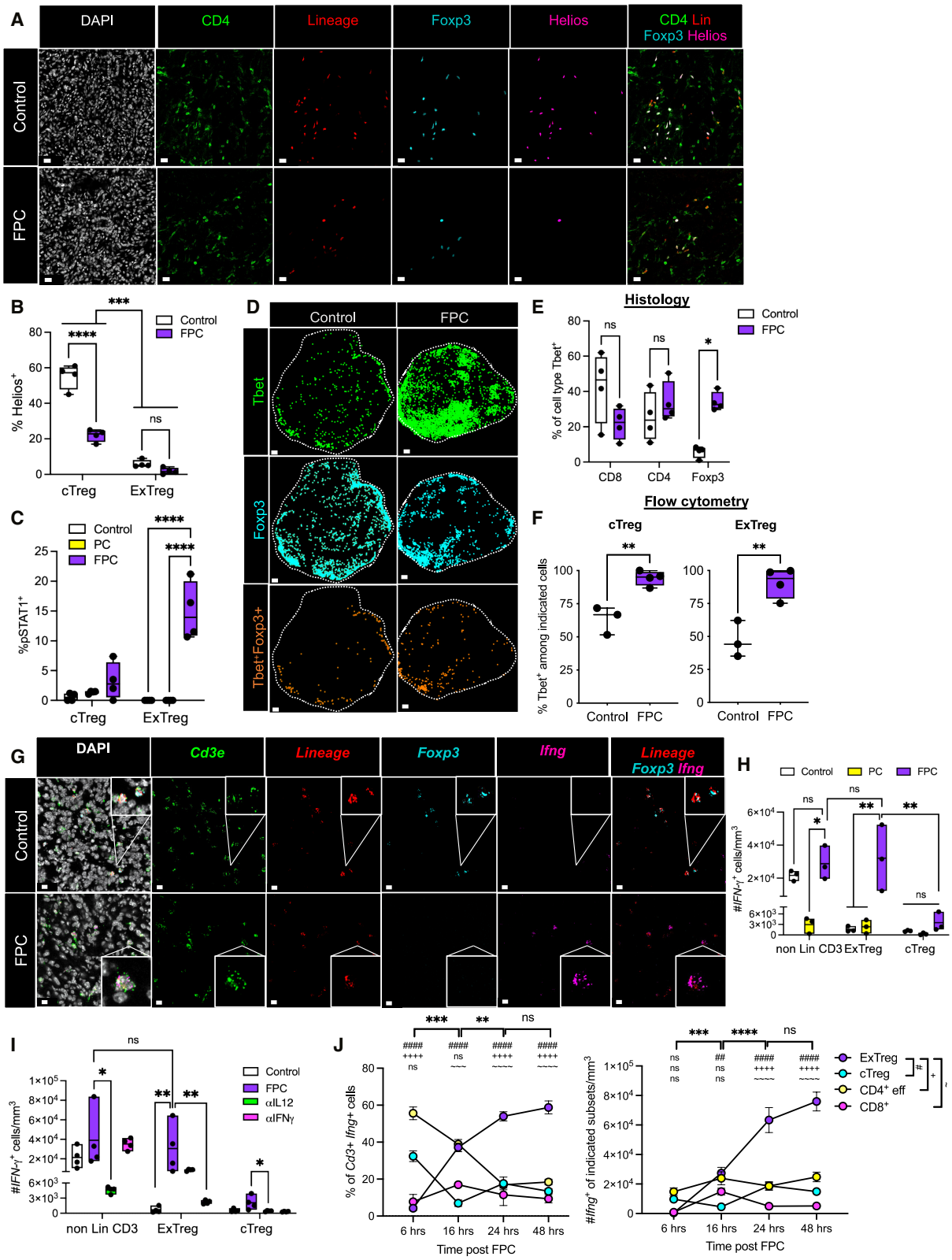

Figure 4. Treg cells acquire a Th1 IFN-γ-producing phenotype after αCD40 therapy

(A and B) Tumors from Foxp3-lineage mice were assessed for Helios by IF (A) and quantified in (B).

(C) Quantification of IF staining of pSTAT1 expression from Figure S4B among lineage subsets after treatment.

(legend continued on next page)

Please cite this article in press as: Maltez et al., Agonistic anti-CD40 antibody treatment converts resident regulatory T cells into activated type 1 effectors within the tumor microenvironment, Immunity (2026), https://doi.org/10.1016/j.immuni.2026.03.011

T cell compartment (Figure 4H). This emphasizes the substantial contribution of ExTreg cells to overall IFN-γ production within the TME after αCD40. Although the number of *Ifng*$^+$ cTreg cells in the TME did not significantly increase with treatment status (Figure 4H), we observed a modest increase in the proportion of those that expressed *Ifng*$^+$ after CD40 stimulation (Figure S4J, left, note axis), reflecting the Th1-skew among the small number of cTreg cells that remained in the TME after FPC. In contrast, PC-treated mice displayed no increase in *Ifng*$^+$ cells within either cTreg or ExTreg cells vs. control-treated mice (Figures 4H and S4J). Antibody blockade of the IL-12/IFN-γ axis abrogated *Ifng* transcripts within both cTreg and ExTreg cells (Figures 4I and S4K), again underscoring the dependence upon the type 1 cytokine axis for these Foxp3-lineage cell changes. To complement our RNAscope findings, we examined ExTreg cells for IFN-γ protein by flow cytometry (Figure S4L), the results of which were consistent with the RNAscope findings of a substantial *Ifng*$^+$-producing ExTreg cell population.

The dual role of IFN-γ as a requirement for both ExTreg cellular development and principal effector cytokine led us to question the identity of the initial IFN-γ-producing cell(s) within the TME. We examined *Ifng*$^+$ expression in T cell subsets over time, noting significantly higher contributions from cTreg and CD4$^+$ T eff cells very early post-αCD40 (Figures 4J left and S4M). At 6 h post-αCD40, CD3$^+$ T cells accounted for 97% of *Ifng* production, with CD4$^+$ T eff cells (55.6%) and cTreg cells (32.4%) as the dominant sources (Figure S4M). Numerical assessments confirmed that the initial sources of *Ifng*$^+$ expression are cTreg and CD4$^+$ T eff cells (Figure 4J, right). By 16 h post-αCD40, ExTreg cells represented a substantial source of *Ifng*, and by 24–48 h, *Ifng*$^+$ ExTreg cells surpassed all other CD3$^+$ T cells, including CD4$^+$ T eff cells (Figure 4J, right). Combined, these data suggest that conventional CD4$^+$ T eff and cTreg cells initiate IFN-γ production and a skew toward a Th1-like program following αCD40. This resulted in ExTreg cell generation, with the feedforward mechanism of the IFN-γ/IL-12 axis promoting Th1-like functions by ExTreg cells as seen by 16 h after αCD40 (Figure 4J).

CXCL9 chemokine axis correlates with spatial redistribution of Treg cells

The localization of ExTreg cells to the tumor border was a prominent feature in the TME after FPC. The IFN-γ-inducible C-X-C chemokine ligand (CXCL)9-CXCR3 chemokine axis can dictate cellular positioning during infection[67] and in the TME,[68–70] potentially aligning with the immuno-landscape of the PDAC TME. Our hypothesis was that a proximity-based signaling cascade initiated by αCD40-stimulated cDC1s might underlie the edge localization of ExTreg cells. We first examined cytokine/chemokine production after αCD40 and found that *Cxcl9*-producing cells increased over 48 h, concurrent with an increase in *Ifng*$^+$ cells (Figures 5A and 5B). *Ifng*$^+$ and *Cxcl9*$^+$ cells showed an increase in proximity over time, from an initial median separation distance of 35 to just 2 μm by 16 h and staying between 4 and 5μm from 24 h on (Figure 5C).

These proximity analyses suggested that the tumor periphery might be especially immunologically active, prompting a more detailed spatial analysis. Our initial observations of altered Treg cells in the TME included a spatial redistribution (Figure 1D). cTreg cell distance to tumor edge 48 h after αCD40 revealed a concentration of Treg cells within the range of 200–300 μm, and we defined the tumor "periphery" as within 250μm of the tumor edge, while the region beyond 250μm of the tumor edge was defined as tumor "center." We observed low baseline densities of *Ifng*$^+$ and *Cxcl9*$^+$ cells in both the periphery and center of tumors in control-treated mice (Figure 5D), whereas after αCD40, there was an increase in the density of *Cxcl9*$^+$ cells and *Ifng*$^+$ cells in the tumor periphery compared with the center (Figure 5D).

Given that CXCL9 expression by cDC1s is linked to the recruitment of CXCR3$^+$ T cells within the tumor site,[67,70,71] we hypothesized that cDC1s recruit T cells to the tumor border. Indeed, αCD40-induced Treg cell localization to the tumor edge coincided with increased localization of cDC1s (defined as CD3$^-$CD11b$^-$CD11c$^+$CD103$^+$MHC II$^+$ cells) to the same peripheral tumor region (Figures 5E and 5F). As a result, cDC1s were closer to both cTreg and ExTreg cells in Foxp3-lineage mice receiving FPC vs. control treatment (Figure S5A). We also observed that *Cd40*$^+$ cDC1s and *Cxcl9*$^+$ cDC1s were increased at the tumor periphery vs. center after αCD40 therapy (Figure 5G).

A larger proportion of cTreg and ExTreg cells expressed *Cxcr3* relative to non-Treg T cells and increased expression of this chemokine receptor over time even in control-treated mice (Figure S5B), which could predispose Foxp3-lineage cells for responsiveness to CXCL9 chemotactic signals. By 48 h after αCD40, nearly all Foxp3-lineage$^+$ cells positioned in the tumor periphery expressed *Cxcr3*$^+$ (Figure S5C), with ExTreg cells as the most abundant *Cxcr3*$^+$ T cell subset (Figure 5H). This was mirrored by an enrichment in the density of *Cxcr3*$^+$ T cells at the periphery vs. center, dominated by the Foxp3-lineage$^+$ cells and specifically ExTreg cells (Figure S5D). We determined the number of Foxp3-lineage cells within 10μm of a *Cxcl9*$^+$ DC (Figures 5I–5K and S5E), a range suggesting these two cell populations may be in direct membrane-membrane communication. Indeed, we found that the majority of *Cxcr3*$^+$ T cells within 10μm of a *Cxcl9*-producing cDC1 comprised cTreg and ExTreg cells

(D and E) Foxp3/Tbet dual fluorescent reporter mice (not lineage) were treated as in Figure 1A, and tumors were analyzed for expression of Tbet reporter among the indicated T cell subsets.

(F) Tumors from Foxp3-lineage mice were treated as in (A) and lineage subsets analyzed by flow cytometry for expression of Tbet among live, CD45$^+$CD3$^+$CD4$^+$ T cells.

(G–J) Distribution of indicated Foxp3-lineage T cell subsets among *Cd3*$^+$*Ifng*$^+$ cells in (G) is quantified in (H) for mice receiving the indicated treatments. (J) Proportion (left) and density (right) of T cell subsets among *Cd3*$^+$*Ifng*$^+$ cells over time. Data represent 2–3 experiments with n = 3–5 mice per group; each symbol represents an individual mouse (B, C, E, F, H, and I) or mean of the group (J). Boxplots: median + IQR, whiskers indicate range (B, C, E, F, H, and I) or the standard error of the mean (J). For analysis, (J) had 3 mice/group/time point. Scale bars: 15 μm for tumor ROI (A and G), 200 μm for whole tumors (D), dotted line indicates tumor edge (D). Stats: two-way ANOVA (B and J), one-way ANOVA (B, C, E, H, and I), both with Tukey's post-test, unpaired t test (G and J), or paired t test (F). Significance: $^*p < 0.05$, $^{**}p < 0.01$, $^{***}p < 0.001$, $^{****}p > 0.0001$.

Please cite this article in press as: Maltez et al., Agonistic anti-CD40 antibody treatment converts resident regulatory T cells into activated type 1 effectors within the tumor microenvironment, Immunity (2026), https://doi.org/10.1016/j.immuni.2026.03.011

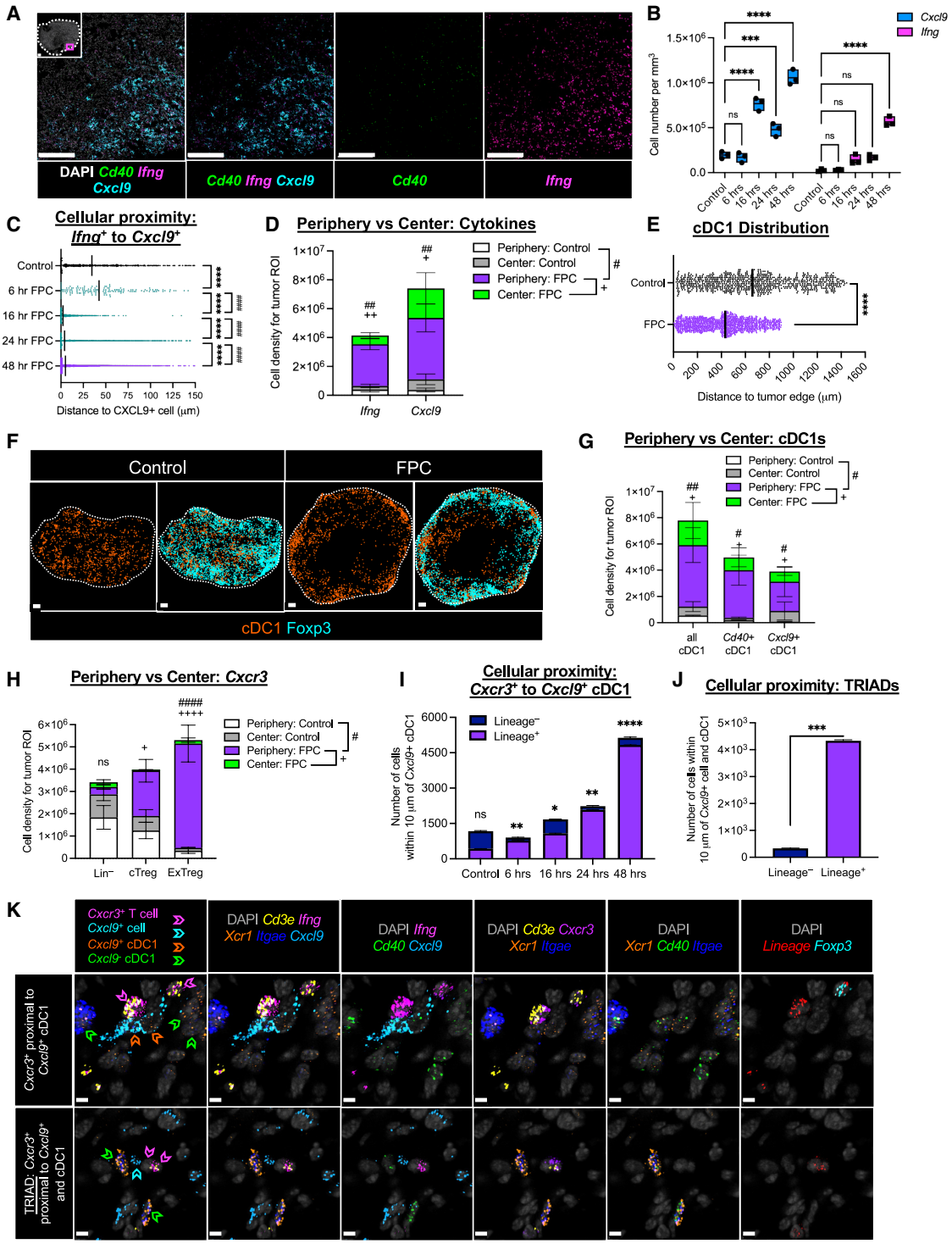

Figure 5. IFN-γ/CXCL9 chemokine axis correlates with post-therapy immune cell positioning

Foxp3-lineage mice were treated as in Figure 3

(A) RNAscope images of an FPC-treated tumor and an inset highlighting the zoom placement within the TME.

(B and C) Quantifications of *Cxcl9*$^+$ and *Ifng*$^+$ cells in the TME (B) and their cellular proximity, both over time.

(D and E) Cell density was calculated for the indicated cytokine-producing cell subsets in control vs. FPC-treated mice. Tumor ROI descriptions for periphery vs. center in main text.

(F and G) Segmented images of cDC1s (CD3$^-$CD11b$^-$CD11c$^+$CD103$^+$MHC II$^+$) from WT mice treated as in Figure 1A (F), with distribution quantifications (G).

(H) Stacked bar graph indicating the T cell subsets among *Cd3*$^+$ *Cxcr3*$^+$ cells.

(legend continued on next page)

Please cite this article in press as: Maltez et al., Agonistic anti-CD40 antibody treatment converts resident regulatory T cells into activated type 1 effectors within the tumor microenvironment, Immunity (2026), https://doi.org/10.1016/j.immuni.2026.03.011

by 6 h after αCD40, both by number (Figure 5I) and proportion (Figure S5F).

Our spatial profiling revealed a substantial number of *Cxcl9*$^+$ cells that lacked expression of *Cd40*, *Itgae*, *Xcr1*, and *Cd3* and that were not cDC1s (Figure S5G). Given the potential for these (non-cDC1) *Cxcl9*$^+$ cells to recruit *Cxcr3*$^+$ T cells, we evaluated the number of events where *Cxcr3*$^+$ cells were within 10μm of both a cDC1 and a *Cxcl9*$^+$ non-cDC1 cell. These putative "triads," where *Cxcr3*$^+$ T cells were within 10 μm of both a cDC1 and a *Cxcl9*$^+$ non-cDC1, represented an additional site at which antigen presentation could involve a *Cxcl9*$^-$ cDC1 and a *Cxcr3*$^+$ ExTreg cell recruited via the nearby *Cxcl9*$^+$ non-cDC1 (Figures 5J and 5K, TRIAD). Approximately half of all *Cxcr3*$^+$ Foxp3-lineage$^+$ cells in the TME were in triads vs. <10% of *Cxcr3*$^+$ non-Foxp3-lineage CD3$^+$ T cells (Figure S5H). In total, 81% of *Cxcr3*$^+$ Foxp3-lineage$^+$ T cells were detected either within 10μm of a cDC1 or within a triad 48 h after αCD40 vs. <8% of non-lineage T cells (Figures S5F and S5H). Given that nearly 75% of both cTreg and ExTreg cells expressed *Cxcr3* at this time point (Figure S5B), these data highlight DC-Treg interactions at the tumor border edge in the TME.

Nuclear localization of NFAT1 indicates active TCR signaling among ExTreg cells

Peptide-loaded major histocompatibility complex class II (MHC class II) (pMHC) mediates antigen-specific interactions between DCs and CD4$^+$ T cells.[40] Thus, we sought to determine the contribution of pMHC class II-TCR interactions to Treg cell reduction after FPC. WT mice received an MHC class II-blocking antibody beginning 2 days before the start of FPC. MHC class II blockade abrogated both cTreg cellular loss and tumor edge localization of residual Treg cells and cDC1s in FPC-treated mice (Figure 6A; quantified in Figures 6B–6D). Furthermore, the proximity of cDC1s and Treg cells after FPC in WT mice was lost in FPC + MHC class II blockade-treated mice (Figure 6E). These data support the notion that cDC1s may actively engage Treg cells at the tumor site during the period of Treg cellular plasticity induced via αCD40.

Although we hypothesize that cDC1s directly stimulate Treg cells in the PDAC TME after αCD40, it has been impossible using available methods to assess antigen reactivity on a single-cell basis in a polyclonal T cell response *in situ*. The nuclear translocation of nuclear factor of activated T cells (NFAT1) due to sustained cytosolic Ca^{2+} is a well-characterized feature of TCR-dependent signaling.[72] NFAT1 nuclear translocation occurs rapidly—within minutes of antigen recognition—but is reversed within 40 min following cessation of TCR engagement.[73–75] We therefore measured cytosolic vs. nuclear NFAT (NFAT1cyt vs. NFAT1nuc) in T cells in fixed tissue samples to gain insight into ongoing T cell antigen recognition. To validate antigen-specific NFAT1 nuclear translocation, we used an OT-II adoptive transfer system and confirmed nuclear NFAT1 (NFAT1nuc$^+$) localization in OT-II T cells within the TdLN of an OVA-expressing tumor (Figures S6A and S6B), with minimal NFAT1nuc$^+$ in OT-II T cells in a WT, non-OVA-expressing tumor (Figure S6B).

We next applied this method to the PDAC TME where the Treg cellular antigens remain undefined. We detected NFAT1nuc within both cTreg and ExTreg cellular compartments as early as 6 h after αCD40, with a progressive increase in NFAT1nuc$^+$ ExTreg cells over time (Figures 6F and 6G). By 48 h after αCD40, FPC-treated mice exhibited increased numbers of NFAT1nuc$^+$ cells within both the ExTreg and CD4$^+$ T eff cell compartments, compared with controls (Figures 6H and S6C). Although the absolute number of NFAT1nuc$^+$ ExTreg cells was not significantly different from that of NFAT1nuc$^+$ CD8$^+$ or CD4$^+$ non-Treg T eff cells after FPC (Figure 6H), ExTreg cells represented the largest proportional contribution to the total NFAT1nuc$^+$ T cell pool beginning 16 h after αCD40 (Figure 6I). This mirrored the acquisition of *Ifng* in T cells (Figure 4I), where beginning 16 h post αCD40, ExTreg cells constituted a large proportion of antigen-specific, antigen-stimulated, cytokine-producing T cells.

Using our NFAT1 visualization and our high-multiplex immunofluorescence (IF) methodology (IBEX, iterative bleaching extends multiplexity),[76] we interrogated the spatial aspects of TCR-engaged T cell subsets within the TME of FPC-treated mice. We found NFAT1nuc$^+$ ExTreg cells concentrated at the tumor edge (Figures 6J and 6K), and a similar edge preference was observed for NFAT1nuc$^+$CD4$^+$ non-Treg cells (Figure 6K) or NFAT1nuc$^+$ cTreg cells (Figure 6K) but not in NFAT1nuc$^+$CD8$^+$ T cells (Figure 6K).

We next assessed cellular proximity and found that NFAT1nuc$^+$ cells were closer to cDC1s than NFAT1cyt$^+$ cells (Figures 6J and 6L). Consistent with our expectation that NFAT1nuc localization reflected *bona fide* TCR signaling, MHC class II-expressing cells co-localized in the tumor periphery with cDC1s, cTreg cells, and ExTreg cells (Figure S6E), and MHC class II blockade prevented NFAT1nuc localization among T cell subsets (Figure S6F). Additionally, the spatial proximity of cDC1s and Treg cell subsets in the PDAC TME correlated with NFAT1nuc$^+$ and *Ifng* expression among Foxp3-lineage cells (Figure S6G) and ultimately, with the conversion of cTreg to ExTreg cells.

αCD40 induces Th1-like Treg cells that are peripherally localized in patient tumors

Agonistic αCD40 is one of the few immunotherapies showing early promise against PDAC in the clinic, with αCD40/chemotherapy advancing after a successful stage II trial.[17] We previously conducted a stage Ib/II clinical trial investigating neoadjuvant αCD40 (NCT02588443)[15] and performed multiplexed immunohistochemistry (mIHC) on the resected tumor samples 12 days after αCD40 treatment.[14] Patient tumors show evidence of type 1 inflammation after αCD40, including an increased IFN-γ signature, enrichment of activated APCs

(I–K) Time course quantification of *Cxcr3*$^+$*Cd3*$^+$ T cell proximity to *Cxcl9*$^+$ cDC1s (defined as: *Cd3*$^-$*Itgae*$^+$*Xcr1*$^+$), after CD40 (I), or to TRIADS comprising a *Cxcl9*$^+$ non-cDC1 and *Cxcl9*$^-$ cDC1 (J), with images (K). Data represent 2 experiments with n = 3–5 mice/group; each symbol represents an individual mouse (B) or cell (C and E); lines indicate the median and error bars indicate the standard error of the mean (SEM). (C–E and G–J) had 3 mice/group. Scale bars: 250 μm (A), 500 μm in inset (A), 200 μm (F), and 4 μm (K); dotted line indicates tumor border. Stats: two-way ANOVA (B, D, and G–I), one-way ANOVA (C), both with Tukey's post-test, or unpaired t test (E and J). Significance: $^*p < 0.05$, $^{**}p < 0.01$, $^{***}p < 0.001$, $^{****}p < 0.0001$.

Please cite this article in press as: Maltez et al., Agonistic anti-CD40 antibody treatment converts resident regulatory T cells into activated type 1 effectors within the tumor microenvironment, Immunity (2026), https://doi.org/10.1016/j.immuni.2026.03.011

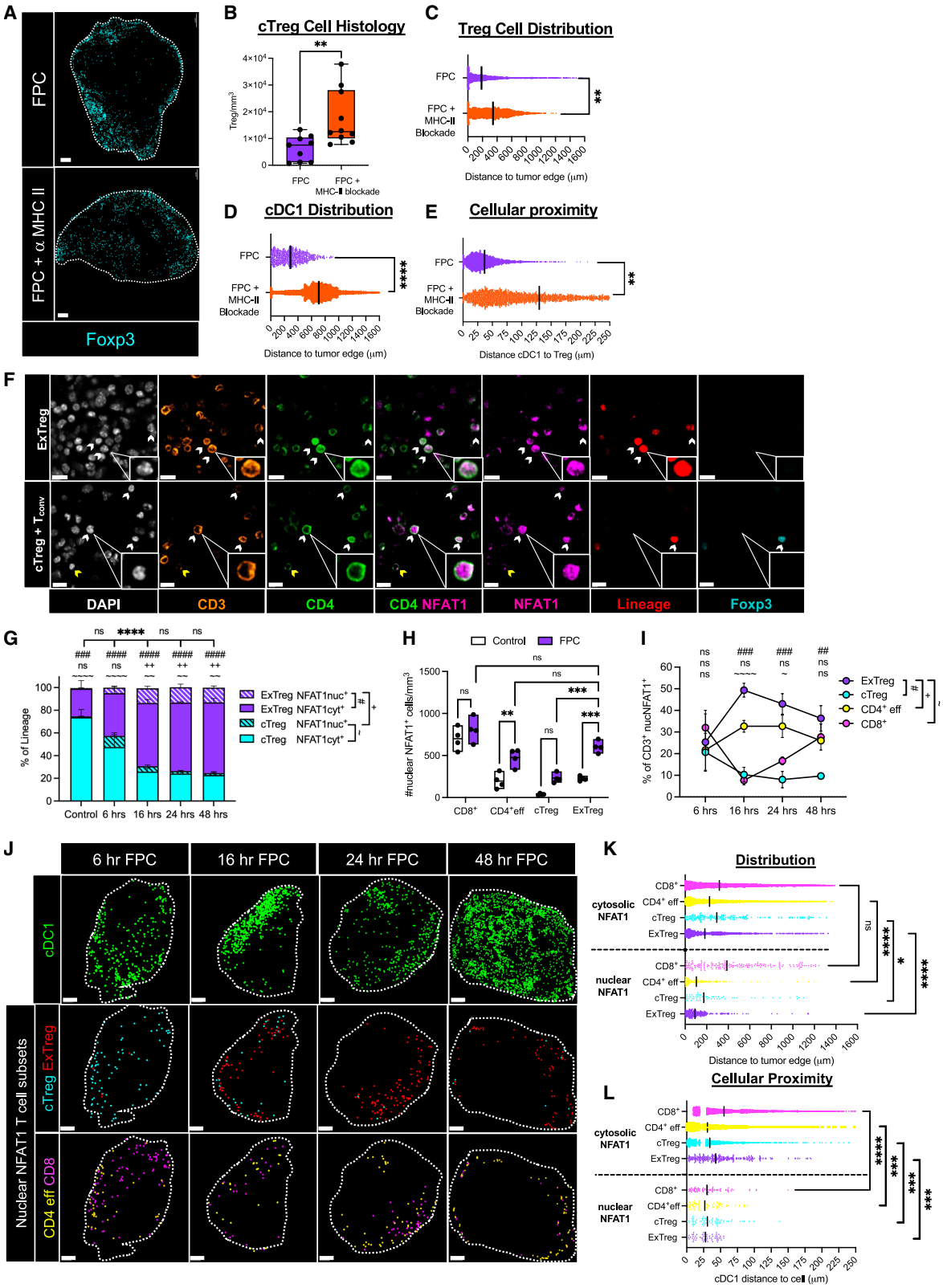

Figure 6. NFAT1 translocation reports TCR signaling by T cells within the polyclonal TME population

(A–E) Tumor-bearing WT mice were treated as in Figure 1A, ±MHC class II-blocking antibody beginning on day 2 before therapy. Segmented images shown in (A), with quantification of total numbers (B), localization of Treg cells (C) or cDC1s (D), and proximity between Treg cells and cDC1s (E).

(legend continued on next page)

Please cite this article in press as: Maltez et al., Agonistic anti-CD40 antibody treatment converts resident regulatory T cells into activated type 1 effectors within the tumor microenvironment, Immunity (2026), https://doi.org/10.1016/j.immuni.2026.03.011

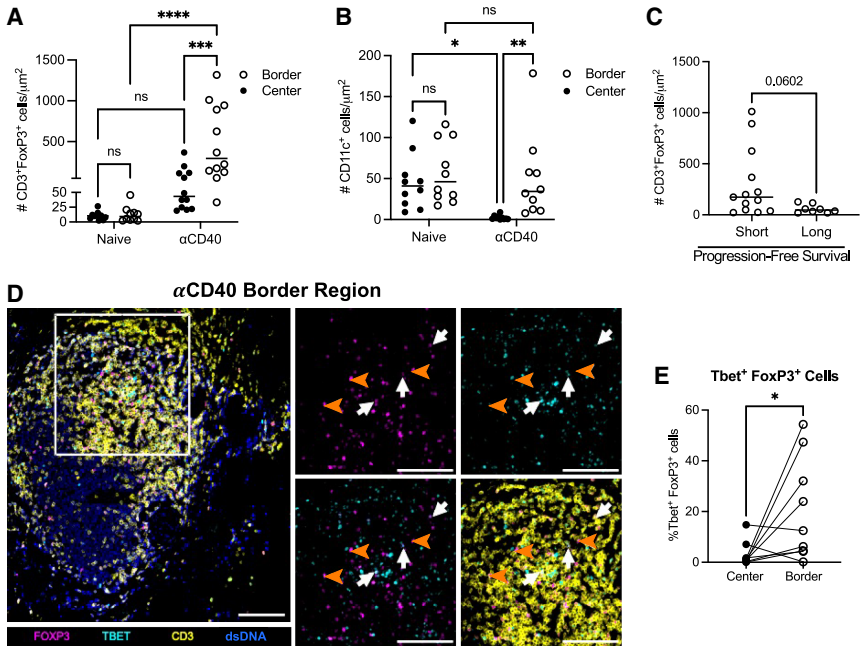

Figure 7. Human neoadjuvant agonistic anti-CD40 treatment is associated with increased Tbet$^+$ Foxp3$^+$ T cells at tumor border

(A–E) Resected PDAC samples from treatment-naive or neoadjuvant agonistic CD40-treated patients (12 days prior) were assessed by mIHC. Treg cells (CD45$^+$CD3$^+$CD8$^-$Foxp3$^+$ cells) (A and C–E) or DCs (CD45$^+$CD3$^-$CD20$^-$CD68$^-$CD11c$^+$ HLA-DP$^+$ cells) (B) were quantified in pathologist-defined center (>0.5 mm from tumor edge) or border (within 0.5 mm of tumor edge). Neoadjuvant CD40-treated patients were stratified by DFS for Treg cell density, indicated as "short progression-free survival" or "long progression-free survival" (C). Tumor center/border regions among CD40-neoadjuvant-treated patients were assessed for Tbet expression among CD45$^+$CD3$^+$CD8$^-$Foxp3$^+$ cells (D) and quantified in (E). Tbet$^-$Foxp3$^+$ cells are orange carets, while Tbet$^+$Foxp3$^+$ cells are white arrows. Analysis by two-way ANOVA with Fisher's post-test (A and B), unpaired *t* test (C), or paired *t* test (E). Significance: indicated (C), * $p < 0.05$, ** $p < 0.01$, *** $p < 0.001$, *** $p < 0.0001$.

(including DCs), and Th1-like CD4 T cells in the TME vs. baseline or untreated tumors,[14–16] supporting the conclusion that some mechanisms of CD40 stimulation promoting type 1 inflammation are conserved between mice and patient PDAC TMEs. The potential impact of αCD40 on the spatial distribution in the TME has not been investigated, but we hypothesized that Tbet expression could be used as a metric of Th1-like Treg cells in patient tumors and compared tumor sections from neoadjuvant-αCD40-treated patients with an atlas of tumor samples from treatment-naive patients[77] via an mIHC panel including markers for CD3$^+$ T cells and Foxp3$^+$ subsets.

Using pathologist-defined annotations, specific regions of interest (ROIs) oriented either intratumorally (center) or at the tumor border ("border") were identified. We previously reported that neoadjuvant CD40-agonist treatment correlates with increased T cell-infiltrated TMEs, as compared with treatment-naive samples, as observed here (Figure 7A). However, the density of Foxp3$^+$ T cells was increased in tumor border vs. center regions in samples from αCD40-treated, but not treatment-naive, patients (Figure 7A). We also observed an enrichment of MHC class II$^+$ (human leukocyte antigen [HLA]-DP$^+$) DCs at the tumor border vs. center after αCD40 (Figure 7B), consistent with the peripheral localization of DCs in the mouse PDAC TMEs after αCD40. To assess the correlation between Treg cells and survival, we stratified neoadjuvant αCD40-treated patients by disease-free survival (DFS), using the median survival of 9.8 months as the threshold. We observed that αCD40-treated patients with long DFS (≥9.8 months) had a trend toward lower densities of Foxp3$^+$CD3$^+$ T cells in the TME, as compared with patients with short DFS (<9.8 months) (Figure 7C). This striking pattern of Treg cell (and DC) accumulation or retention at the tumor border with a relative loss in the center, coupled with the reduced frequency of cTreg cells in patients with long DFS, suggested that αCD40 stimulation may impact the Treg cells and DCs in patient PDAC TMEs.

The proportion of Tbet$^+$Foxp3$^+$ T cells was also increased in intratumoral regions from patients treated with αCD40 vs. treatment-naive patients (Figure 7D; quantified in Figure 7E). Tbet$^+$Foxp3$^+$ cells were concentrated in border (vs. intratumoral center) regions of tumor samples in patients that received agonistic CD40 (Figure 7E), consistent with the conclusion that αCD40 skews Treg cells toward a Th1-like cell subset along with reorganization of Treg cells and DCs toward the outer regions of the patient PDAC TMEs. Together, these indicate a destabilization among Treg cells with a concomitant increase in Tbet expression and DC proximity after αCD40 in both mouse and patient TMEs.

DISCUSSION

Overcoming Treg cell-mediated suppression is a major goal of cancer immunotherapy. The immunosuppressive Treg cell state

(F–L) Tamoxifen-inducible Foxp3-lineage tracing mice were used for IBEX staining (Methods). (F) Images depict nuclear NFAT1 (NFAT1nuc$^+$; white arrows) and cytoplasmic NFAT1 (NFATcyt$^+$, yellow arrows). NFAT1nuc$^+$ cell quantification in (G) cTreg and ExTreg cell proportions over time, (H) subset proportions ± FPC, and (I) subset proportions over time. (J–L) Images of NFAT1nuc$^+$ over time (J), T cell subset distribution (K), and proximity to cDC1 cells (L). Data represent 2 experiments with 3–5 mice/group; symbol represents an individual mouse (B and H) or cell (C–E, K, and L), lines indicate median, whiskers indicate range (B), and error bars indicate standard error of the mean (G and I). (B–E) Same experiment, *n* in (B); (G) 4 mice/group; (I) 3 mice/group; (K and L) same experiment, with 3 mice/group. Scale bars: 5 μm (A) or 300 μm (A and J). Stats: unpaired *t* test (B–E), two-way ANOVA (G–I), one-way ANOVA (K and L), both with Tukey's post-test. Significance: *$p < 0.05$, **$p < 0.01$, ***$p < 0.001$, ****$p < 0.0001$.

Please cite this article in press as: Maltez et al., Agonistic anti-CD40 antibody treatment converts resident regulatory T cells into activated type 1 effectors within the tumor microenvironment, Immunity (2026), https://doi.org/10.1016/j.immuni.2026.03.011

in the tumor is established and maintained via unstable DC-Treg cellular interactions,[73,78,79] raising the following question: can Treg cells be reprogrammed in the TME? Here, we show that CD40 stimulation of cDC1s leads to substantial loss of Foxp3$^+$ Treg cells and spatial reorganization of the immuno-landscape. IL-12 and IFN-γ signaling evoked by αCD40-stimulated DCs led to cTreg cell conversion into IFN-γ-producing Tbet$^+$ ExTreg cells within 16 h, and these ExTreg cells represented the highest fraction of active antigen-dependent signaling among all T cells in the TME.

Our findings contrast with αCTLA-4-driven Treg cell depletion via ADCC. Here, ExTreg cells fully lost Foxp3 expression and displayed a mature type 1 phenotype after CD40 stimulation, marked by downregulation of Helios and the upregulation of Tbet and IFN-γ. Our lineage tracing data also excluded transient Foxp3 expression as responsible for our observations.[39,80,81] The self-perpetuating inflammatory TME generated by αCD40 may provide a unique environment for TCR-stimulated cTreg cell conversion to ExTreg cells that may contribute to effective anti-tumor immunity through type 1 cytokine production.

The Foxp3$^-$ ExTreg cells described here are distinct from cTreg cells that retain detectable Foxp3 expression but acquire Th1-like features. In some settings, Tbet$^+$Foxp3$^+$ Treg cells gain Th1-like effector function, including IFN-γ-production after infection[48] or in the TME upon inhibition of mucosa associated lymphoid tissue lymphoma translocation protein-1 (MALT-1),[64] loss of Treg-intrinsic IL-33 expression,[82] IL-6-induced reprogrammed Treg cells,[49] or induction of IFN-γ/neuropilin (Nrp)1-mediated Treg cellular "fragility,"[83] although in the latter study, there was no evidence of ExTreg cell generation.[83] Thus, "fragile" or reprogrammed cTreg cellular subsets are transcriptionally and phenotypically distinct from the ExTreg cells described in our study, highlighting the nuances of Treg cellular plasticity.

Using an *in situ* technique to visualize nuclear translocation of NFAT1 after TCR engagement,[72] we examined the differential requirements for ExTreg cells vs. reprogrammed/fragile cTreg cells within the same hyperlocal microenvironment. The low frequency of nucNFAT1$^+$ cTreg cells after CD40 stimulation of DCs suggests the followingt: (1) ExTreg cellular conversion may require signaling via the TCR, and (2) cTreg cells detecting higher antigen affinity or amount may preferentially undergo ExTreg cellular conversion. In the absence of any known antigens, interrogating *bona fide* antigen-reactive NFAT1nuc$^+$ within the PDAC TME could enable diagnostic distinction between a "cold" tumor that lacks T cell infiltration and a tumor with ongoing "active" immune responses.

NFAT1nuc$^+$ T cells were predominantly positioned toward the tumor edge, where ExTreg cells were in close proximity to cDC1s—a distribution mirrored in patient samples. These same tumor border regions also include Tbet$^+$Foxp3$^+$ Treg cells, consistent with the Th1-skewing of cTreg cells seen in the mouse model and highlighting the enhanced Treg-DC proximity at the tumor periphery in patient tumors. This key feature of cTreg-to-ExTreg cellular conversion is likely driven by CXCL9-CXCR3 signaling,[68] which may be related to IFN-γ-induced *Cxcl9* production by cDC1s and other border-associated cells to recruit and position *Cxcr3*$^+$ cTreg and ExTreg cells within the tumor periphery niche.

The rapidity of ExTreg cell generation after αCD40 indicates that Foxp3$^+$ cells may represent a reprogrammable subset of T cells within the TME. Rather than assuming that an accumulation of Treg cells is irreversibly linked to a poor prognostic outcome, Treg cell plasticity might instead be leveraged to improve patient outcomes. We propose that simultaneously reducing the suppressive capabilities of cTreg cells and increasing the type 1 ExTreg cells within the TME may make significant positive contributions to anti-tumor immunity. The power to change the allegiance of a pro-tumoral, immunosuppressive cell subset, even if fleeting, could provide critical early modifications in the TME, which dictate therapeutic responsiveness.

Limitations of the study

Our study has limitations, including incomplete resolution regarding the suppressive capacity or functional implications of residual Foxp3$^+$ cTreg cells and newly generated ExTreg cells. In our model, a significant proportion of the remaining cTreg cells produced *Ifng*, potentially representing transitional states. Future studies could use adoptive transfer models, tumor organoids systems, or genetic restriction of IFN-γ production to Foxp3-lineage cells to assess the role of ExTreg cells in tumor control. Our findings are in keeping with the observation that a Th1-like ExTreg cell population, showing increased expression of *IFNG*, is observed in lung adenocarcinomas with a clinical response to αPD-1 therapy.[54]

RESOURCE AVAILABILITY

Lead contact

Further information and requests for resources and reagents should be directed to and will be fulfilled by the lead contact, Katelyn T. Byrne (byrneka@ohsu.edu).

Materials availability

This study did not generate new unique reagents.

Data and code availability

Data sharing is not applicable to this article as no datasets for which public repositories exist were generated or analyzed during the current study.

ACKNOWLEDGMENTS

We thank the site investigators for the CD40 clinical trial and the Brenden-Colson Center for Pancreatic Care, especially Drs. Dove Keith and Jason Link. We also thank the Byrne, Germain, and Vonderheide labs for helpful conversations and are especially grateful to Andrea Radtke for advice and establishing methods used herein. This research was supported (in part) by the Intramural Research Program of the National Institutes of Health (NIH). The contributions of the NIH author(s) were made as part of their official duties as NIH federal employees, are in compliance with agency policy requirements, and are considered Works of the United States Government. However, the findings and conclusions presented in this paper are those of the author(s) and do not necessarily reflect the views of the NIH or the U.S. Department of Health and Human Services. This work was also supported by NIH NCI grants R01CA229803 (R.H.V.) and a Bench-to-Bedside supplement (R.H.V. and R.N.G.), NCI T32 CA254888 (K.E.B.), NIGMS PRAT Fellowship Fi2GM133442 (V.I.M.), the Parker Institute for Cancer Immunotherapy (R.H.V. and K.T.B.), and generous start-up funding from the Knight Cancer Institute and the Brenden-Colson Center for Pancreatic Care at OHSU (K.T.B.).

AUTHOR CONTRIBUTIONS

Conceptualization, V.I.M., R.N.G., and K.T.B.; formal analysis, V.I.M. and K.T.B.; funding acquisition, V.I.M., R.H.V., R.N.G., and K.T.B.; investigation, V.I.M., K.P.G., B.C., M.E.H., C.A., R.S., Q.L., K.E.B., S.S., and K.T.B.;

Please cite this article in press as: Maltez et al., Agonistic anti-CD40 antibody treatment converts resident regulatory T cells into activated type 1 effectors within the tumor microenvironment, Immunity (2026), https://doi.org/10.1016/j.immuni.2026.03.011

methodology, V.I.M., S.S., L.M.C., R.N.G., and K.T.B.; resources, R.C.S., L.M.C., R.H.V., R.N.G., and K.T.B.; supervision, R.N.G. and K.T.B.; visualization, V.I.M., K.E.B., and K.T.B.; writing – original draft, V.I.M., R.N.G., and K.T.B.; and writing – review and editing, all authors.

DECLARATION OF INTERESTS

R.C.S. is a consultant for Revolution Medicine and Larkspur Bioscience and received research support from Cardiff Oncology and AstraZeneca. L.M.C. has received reagent support from Cell Signaling Technologies, Syndax Pharmaceuticals, Inc., ZielBio, Inc., and Hibercell, Inc.; holds sponsored research agreements with Prospect Creek Foundation and previously from ZielBio, Inc.; receives grant support from Susan G. Komen Foundation, National Foundation for Cancer Research, and the National Cancer Institute; and is on the Advisory Board for Carisma Therapeutics, Inc., CytomX Therapeutics, Inc., Kineta, Inc., Hibercell, Inc., Cell Signaling Technologies, Inc., Alkermes, Inc., NextCure, Guardian Bio, Dispatch Biotherapeutics, AstraZeneca Partner of Choice Network (OHSU Site Leader), Genenta Sciences, Pio Therapeutics Pty Ltd., and Lustgarten Foundation for Pancreatic Cancer Research Therapeutics Working Group, Inc. R.H.V. is an inventor on licensed patents relating to cancer cellular immunotherapy and cancer vaccines and mutant Kras-specific TCRs; has received consulting fees from Bristol Myers Squibb; and receives royalties from the Children's Hospital Boston for a licensed research-only monoclonal antibody. R.N.G. is a member of the *Immunity* advisory board. K.T.B. receives royalties from the University of Pennsylvania for licensed research cell lines and has received consulting fees from Guidepoint Global.

STAR★METHODS

Detailed methods are provided in the online version of this paper and include the following:

- KEY RESOURCES TABLE
  - Mice
- METHOD DETAILS
  - *In vivo* reagents and treatments
  - Implantation of tumor cell clones
  - OT-II and MC38
  - Subcutaneous tumor growth, regression, and animal survival assessment
  - Tissue section preparation, processing, and immunostaining
  - IBEX
  - Antibodies for Immunofluorescence
  - RNAScope
  - Laser scanning confocal microscopy
  - Image processing, segmentation, and analysis
  - Imaris algorithm for Foxp3 Lineage tumor analyses
  - Flow cytometry of murine tumor samples
  - Multiplexed immunohistochemistry (mIHC) analysis of patient samples
  - Statistical Analysis

SUPPLEMENTAL INFORMATION

Supplemental information can be found online at https://doi.org/10.1016/j.immuni.2026.03.011.

Received: October 15, 2024
Revised: June 11, 2025
Accepted: March 11, 2026

REFERENCES

1. de Visser, K.E., and Joyce, J.A. (2023). The evolving tumor microenvironment: From cancer initiation to metastatic outgrowth. Cancer Cell *41*, 374–403. https://doi.org/10.1016/j.ccell.2023.02.016.
2. Gill, A.L., Wang, P.H., Lee, J., Hudson, W.H., Ando, S., Araki, K., Hu, Y., Wieland, A., Im, S., Gavora, A., et al. (2023). PD-1 blockade increases the self-renewal of stem-like CD8 T cells to compensate for their accelerated differentiation into effectors. Sci. Immunol. *8*, eadg0539. https://doi.org/10.1126/sciimmunol.adg0539.
3. Yokosuka, T., Takamatsu, M., Kobayashi-Imanishi, W., Hashimoto-Tane, A., Azuma, M., and Saito, T. (2012). Programmed cell death 1 forms negative costimulatory microclusters that directly inhibit T cell receptor signaling by recruiting phosphatase SHP2. J. Exp. Med. *209*, 1201–1217. https://doi.org/10.1084/jem.20112741.
4. Chan, W., Cao, Y.M., Zhao, X., Schrom, E.C., Jia, D., Song, J., Sibener, L.V., Dong, S., Fernandes, R.A., Bradfield, C.J., et al. (2023). TCR ligand potency differentially impacts PD-1 inhibitory effects on diverse signaling pathways. J. Exp. Med. *220*, e20231242. https://doi.org/10.1084/jem.20231242.
5. Peggs, K.S., Quezada, S.A., Chambers, C.A., Korman, A.J., and Allison, J.P. (2009). Blockade of CTLA-4 on both effector and regulatory T cell compartments contributes to the antitumor activity of anti–CTLA-4 antibodies. J. Exp. Med. *206*, 1717–1725. https://doi.org/10.1084/jem.20082492.
6. Simpson, T.R., Li, F., Montalvo-Ortiz, W., Sepulveda, M.A., Bergerhoff, K., Arce, F., Roddie, C., Henry, J.Y., Yagita, H., Wolchok, J.D., et al. (2013). Fc-dependent depletion of tumor-infiltrating regulatory T cells co-defines the efficacy of anti–CTLA-4 therapy against melanoma. J. Exp. Med. *210*, 1695–1710. https://doi.org/10.1084/jem.20130579.
7. Marabelle, A., Le, D.T., Ascierto, P.A., Di Giacomo, A.M., De Jesus-Acosta, A., Delord, J.-P., Geva, R., Gottfried, M., Penel, N., Hansen, A.R., et al. (2019). Efficacy of Pembrolizumab in Patients With Noncolorectal High Microsatellite Instability/Mismatch Repair-Deficient Cancer: Results From the Phase II KEYNOTE-158 Study. J. Clin. Oncol. *38*, 1–10. https://doi.org/10.1200/jco.19.02105.
8. French, R.R., Chan, H.T.C., Tutt, A.L., and Glennie, M.J. (1999). CD40 antibody evokes a cytotoxic T-cell response that eradicates lymphoma and bypasses T-cell help. Nat. Med. *5*, 548–553. https://doi.org/10.1038/8426.
9. Diehl, L., den den Boer, A.Th., Schoenberger, S.P., van der van der Voort, E.I.H., Schumacher, T.N.M., Melief, C.J.M., Offringa, R., and Toes, R.E.M. (1999). CD40 activation in vivo overcomes peptide-induced peripheral cytotoxic T-lymphocyte tolerance and augments anti-tumor vaccine efficacy. Nat. Med. *5*, 774–779. https://doi.org/10.1038/10495.
10. Sotomayor, E.M., Borrello, I., Tubb, E., Rattis, F.M., Bien, H., Lu, Z., Fein, S., Schoenberger, S., and Levitsky, H.I. (1999). Conversion of tumor-specific CD4+ T-cell tolerance to T-cell priming through in vivo ligation of CD40. Nat. Med. *5*, 780–787. https://doi.org/10.1038/10503.
11. Li, J., Byrne, K.T., Yan, F., Yamazoe, T., Chen, Z., Baslan, T., Richman, L.P., Lin, J.H., Sun, Y.H., Rech, A.J., et al. (2018). Tumor Cell-Intrinsic Factors Underlie Heterogeneity of Immune Cell Infiltration and Response to Immunotherapy. Immunity *49*, 178–193.e7. https://doi.org/10.1016/j.immuni.2018.06.006.
12. Byrne, K.T., and Vonderheide, R.H. (2016). CD40 Stimulation Obviates Innate Sensors and Drives T Cell Immunity in Cancer. Cell Rep. *15*, 2719–2732. https://doi.org/10.1016/j.celrep.2016.05.058.
13. Morrison, A.H., Diamond, M.S., Hay, C.A., Byrne, K.T., and Vonderheide, R.H. (2020). Sufficiency of CD40 activation and immune checkpoint blockade for T cell priming and tumor immunity. Proc. Natl. Acad. Sci. USA *117*, 8022–8031. https://doi.org/10.1073/pnas.1918971117.
14. Blise, K.E., Sivagnanam, S., Betts, C.B., Betre, K., Kirchberger, N., Tate, B.J., Furth, E.E., Costa, A.D., Nowak, J.A., Wolpin, B.M., et al. (2024). Machine learning links T-cell function and spatial localization to neoadjuvant immunotherapy and clinical outcome in pancreatic cancer. Cancer Immunol. Res. *12*, 544–558. https://doi.org/10.1158/2326-6066.cir-23-0873.
15. Byrne, K.T., Betts, C.B., Mick, R., Sivagnanam, S., Bajor, D.L., Laheru, D.A., Chiorean, E.G., O'Hara, M.H., Liudahl, S.M., Newcomb, C., et al. (2021). Neoadjuvant Selicrelumab, an Agonist CD40 Antibody, Induces Changes in the Tumor Microenvironment in Patients with Resectable

Please cite this article in press as: Maltez et al., Agonistic anti-CD40 antibody treatment converts resident regulatory T cells into activated type 1 effectors within the tumor microenvironment, Immunity (2026), https://doi.org/10.1016/j.immuni.2026.03.011

Pancreatic Cancer. Clin. Cancer Res. *27*, 4574–4586. https://doi.org/10.1158/1078-0432.ccr-21-1047.

16. Padrón, L.J., Maurer, D.M., O'Hara, M.H., O'Reilly, E.M., Wolff, R.A., Wainberg, Z.A., Ko, A.H., Fisher, G., Rahma, O., Lyman, J.P., et al. (2022). Sotigalimab and/or nivolumab with chemotherapy in first-line metastatic pancreatic cancer: clinical and immunologic analyses from the randomized phase 2 PRINCE trial. Nat. Med. *28*, 1167–1177. https://doi.org/10.1038/s41591-022-01829-9.
17. Van Laethem, J.-L.V., Borbath, I., Prenen, H., Geboes, K.P., Lambert, A., Mitry, E., Cassier, P.A., Blanc, J.-F., Pilla, L., Batlle, J.F., et al. (2024). Combining CD40 agonist mitazalimab with mFOLFIRINOX in previously untreated metastatic pancreatic ductal adenocarcinoma (OPTIMIZE-1): a single-arm, multicentre phase 1b/2 study. Lancet Oncol. *25*, 853–864. https://doi.org/10.1016/s1470-2045(24)00263-8.
18. Osorio, J.C., Knorr, D.A., Weitzenfeld, P., Blanchard, L., Yao, N., Baez, M., Sevilla, C., DiLillo, M., Rahman, J., Sharma, V.P., et al. (2025). Fc-optimized CD40 agonistic antibody elicits tertiary lymphoid structure formation and systemic antitumor immunity in metastatic cancer. Cancer Cell *43*, 1902–1916.e9. https://doi.org/10.1016/j.ccell.2025.07.013.
19. Lin, J.H., Huffman, A.P., Wattenberg, M.M., Walter, D.M., Carpenter, E.L., Feldser, D.M., Beatty, G.L., Furth, E.E., and Vonderheide, R.H. (2020). Type 1 conventional dendritic cells are systemically dysregulated early in pancreatic carcinogenesis. J. Exp. Med. *217*, e20190673. https://doi.org/10.1084/jem.20190673.
20. Pandiyan, P., Zheng, L., Ishihara, S., Reed, J., and Lenardo, M.J. (2007). CD4+CD25+Foxp3+ regulatory T cells induce cytokine deprivation–mediated apoptosis of effector CD4+ T cells. Nat. Immunol. *8*, 1353–1362. https://doi.org/10.1038/ni1536.
21. Read, S., Greenwald, R., Izcue, A., Robinson, N., Mandelbrot, D., Francisco, L., Sharpe, A.H., and Powrie, F. (2006). Blockade of CTLA-4 on CD4+CD25+ Regulatory T Cells Abrogates Their Function In Vivo. J. Immunol. *177*, 4376–4383. https://doi.org/10.4049/jimmunol.177.7.4376.
22. Maj, T., Wang, W., Crespo, J., Zhang, H., Wang, W., Wei, S., Zhao, L., Vatan, L., Shao, I., Szeliga, W., et al. (2017). Oxidative stress controls regulatory T cell apoptosis and suppressor activity and PD-L1-blockade resistance in tumor. Nat. Immunol. *18*, 1332–1341. https://doi.org/10.1038/ni.3868.
23. Mellor, A.L., and Munn, D.H. (2004). Ido expression by dendritic cells: tolerance and tryptophan catabolism. Nat. Rev. Immunol. *4*, 762–774. https://doi.org/10.1038/nri1457.
24. Shan, F., Somasundaram, A., Bruno, T.C., Workman, C.J., and Vignali, D.A.A. (2022). Therapeutic targeting of regulatory T cells in cancer. Trends Cancer *8*, 944–961. https://doi.org/10.1016/j.trecan.2022.06.008.
25. Finke, J.H., Rini, B., Ireland, J., Rayman, P., Richmond, A., Golshayan, A., Wood, L., Elson, P., Garcia, J., Dreicer, R., et al. (2008). Sunitinib Reverses Type-1 Immune Suppression and Decreases T-Regulatory Cells in Renal Cell Carcinoma Patients. Clin. Cancer Res. *14*, 6674–6682. https://doi.org/10.1158/1078-0432.ccr-07-5212.
26. Ge, Y., Domschke, C., Stoiber, N., Schott, S., Heil, J., Rom, J., Blumenstein, M., Thum, J., Sohn, C., Schneeweiss, A., et al. (2012). Metronomic cyclophosphamide treatment in metastasized breast cancer patients: immunological effects and clinical outcome. Cancer Immunol. Immunother. *61*, 353–362. https://doi.org/10.1007/s00262-011-1106-3.
27. Guan, X., Hu, R., Choi, Y., Srivats, S., Nabet, B.Y., Silva, J., McGinnis, L., Hendricks, R., Nutsch, K., Banta, K.L., et al. (2024). Anti-TIGIT antibody improves PD-L1 blockade through myeloid and Treg cells. Nature *627*, 646–655. https://doi.org/10.1038/s41586-024-07121-9.
28. Durham, N.M., Nirschl, C.J., Jackson, C.M., Elias, J., Kochel, C.M., Anders, R.A., and Drake, C.G. (2014). Lymphocyte Activation Gene 3 (LAG-3) Modulates the Ability of CD4 T-cells to Be Suppressed In Vivo. PLoS One *9*, e109080. https://doi.org/10.1371/journal.pone.0109080.
29. Zhang, Q., Chikina, M., Szymczak-Workman, A.L., Horne, W., Kolls, J.K., Vignali, K.M., Normolle, D., Bettini, M., Workman, C.J., and Vignali, D.A.A. (2017). LAG3 limits regulatory T cell proliferation and function in autoimmune diabetes. Sci. Immunol. *2*, eaah4569. https://doi.org/10.1126/sciimmunol.aah4569.
30. Curiel, T.J., Coukos, G., Zou, L., Alvarez, X., Cheng, P., Mottram, P., Evdemon-Hogan, M., Conejo-Garcia, J.R., Zhang, L., Burow, M., et al. (2004). Specific recruitment of regulatory T cells in ovarian carcinoma fosters immune privilege and predicts reduced survival. Nat. Med. *10*, 942–949. https://doi.org/10.1038/nm1093.
31. Barsheshet, Y., Wildbaum, G., Levy, E., Vitenshtein, A., Akinseye, C., Griggs, J., Lira, S.A., and Karin, N. (2017). CCR8+FOXp3+ Treg cells as master drivers of immune regulation. Proc. Natl. Acad. Sci. USA *114*, 6086–6091. https://doi.org/10.1073/pnas.1621280114.
32. Chaudhry, A., Samstein, R.M., Treuting, P., Liang, Y., Pils, M.C., Heinrich, J.-M., Jack, R.S., Wunderlich, F.T., Brüning, J.C., Müller, W., et al. (2011). Interleukin-10 Signaling in Regulatory T Cells Is Required for Suppression of Th17 Cell-Mediated Inflammation. Immunity *34*, 566–578. https://doi.org/10.1016/j.immuni.2011.03.018.
33. Turnis, M.E., Sawant, D.V., Szymczak-Workman, A.L., Andrews, L.P., Delgoffe, G.M., Yano, H., Beres, A.J., Vogel, P., Workman, C.J., and Vignali, D.A.A. (2016). Interleukin-35 Limits Anti-Tumor Immunity. Immunity *44*, 316–329. https://doi.org/10.1016/j.immuni.2016.01.013.
34. Sawant, D.V., Yano, H., Chikina, M., Zhang, Q., Liao, M., Liu, C., Callahan, D.J., Sun, Z., Sun, T., Tabib, T., et al. (2019). Adaptive plasticity of IL-10+ and IL-35+ Treg cells cooperatively promotes tumor T cell exhaustion. Nat. Immunol. *20*, 724–735. https://doi.org/10.1038/s41590-019-0346-9.
35. Lainé, A., Labiad, O., Hernandez-Vargas, H., This, S., Sanlaville, A., Léon, S., Dalle, S., Sheppard, D., Travis, M.A., Paidassi, H., et al. (2021). Regulatory T cells promote cancer immune-escape through integrin αvβ8-mediated TGF-β activation. Nat. Commun. *12*, 6228. https://doi.org/10.1038/s41467-021-26352-2.
36. Tang, T., Cheng, X., Truong, B., Sun, L., Yang, X., and Wang, H. (2020). Molecular basis and therapeutic implications of CD40/CD40L immune checkpoint. Pharmacol. Ther. *219*, 107709. https://doi.org/10.1016/j.pharmthera.2020.107709.
37. Zhou, X., Bailey-Bucktrout, S.L., Jeker, L.T., Penaranda, C., Martínez-Llordella, M., Ashby, M., Nakayama, M., Rosenthal, W., and Bluestone, J.A. (2009). Instability of the transcription factor Foxp3 leads to the generation of pathogenic memory T cells in vivo. Nat. Immunol. *10*, 1000–1007. https://doi.org/10.1038/ni.1774.
38. Gerner, M.Y., Kastenmuller, W., Ifrim, I., Kabat, J., and Germain, R.N. (2012). Histo-Cytometry: A Method for Highly Multiplex Quantitative Tissue Imaging Analysis Applied to Dendritic Cell Subset Microanatomy in Lymph Nodes. Immunity *37*, 364–376. https://doi.org/10.1016/j.immuni.2012.07.011.
39. Miyao, T., Floess, S., Setoguchi, R., Luche, H., Fehling, H.J., Waldmann, H., Huehn, J., and Hori, S. (2012). Plasticity of Foxp3+ T Cells Reflects Promiscuous Foxp3 Expression in Conventional T Cells but Not Reprogramming of Regulatory T Cells. Immunity *36*, 262–275. https://doi.org/10.1016/j.immuni.2011.12.012.
40. Ferris, S.T., Durai, V., Wu, R., Theisen, D.J., Ward, J.P., Bern, M.D., Davidson, J.T., Bagadia, P., Liu, T., Briseño, C.G., et al. (2020). cDC1 prime and are licensed by CD4+ T cells to induce anti-tumour immunity. Nature *584*, 624–629. https://doi.org/10.1038/s41586-020-2611-3.
41. Hor, J.L., Whitney, P.G., Zaid, A., Brooks, A.G., Heath, W.R., and Mueller, S.N. (2015). Spatiotemporally Distinct Interactions with Dendritic Cell Subsets Facilitates CD4+ and CD8+ T Cell Activation to Localized Viral Infection. Immunity *43*, 554–565. https://doi.org/10.1016/j.immuni.2015.07.020.
42. Kastenmüller, W., Gerner, M.Y., and Germain, R.N. (2010). The in situ dynamics of dendritic cell interactions. Eur. J. Immunol. *40*, 2103–2106. https://doi.org/10.1002/eji.201040482.
43. Hildner, K., Edelson, B.T., Purtha, W.E., Diamond, M., Matsushita, H., Kohyama, M., Calderon, B., Schraml, B.U., Unanue, E.R., Diamond, M.S., et al. (2008). Batf3 Deficiency Reveals a Critical Role for CD8α+ Dendritic Cells in Cytotoxic T Cell Immunity. Science *322*, 1097–1100. https://doi.org/10.1126/science.1164206.

Please cite this article in press as: Maltez et al., Agonistic anti-CD40 antibody treatment converts resident regulatory T cells into activated type 1 effectors within the tumor microenvironment, Immunity (2026), https://doi.org/10.1016/j.immuni.2026.03.011

44. Hodge-Dufour, J., Marino, M.W., Horton, M.R., Jungbluth, A., Burdick, M.D., Strieter, R.M., Noble, P.W., Hunter, C.A., and Puré, E. (1998). Inhibition of interferon γ induced interleukin 12 production: A potential mechanism for the anti-inflammatory activities of tumor necrosis factor. Proc. Natl. Acad. Sci. USA *95*, 13806–13811. https://doi.org/10.1073/pnas.95.23.13806.

45. Ma, X., Chow, J.M., Gri, G., Carra, G., Gerosa, F., Wolf, S.F., Dzialo, R., and Trinchieri, G. (1996). The interleukin 12 p40 gene promoter is primed by interferon gamma in monocytic cells. J. Exp. Med. *183*, 147–157. https://doi.org/10.1084/jem.183.1.147.

46. Magram, J., Connaughton, S.E., Warrier, R.R., Carvajal, D.M., Wu, C.Y., Ferrante, J., Stewart, C., Sarmiento, U., Faherty, D.A., and Gately, M.K. (1996). IL-12-Deficient Mice Are Defective in IFNγ Production and Type 1 Cytokine Responses. Immunity *4*, 471–481. https://doi.org/10.1016/s1074-7613(00)80413-6.

47. Dalton, D.K., Pitts-Meek, S., Keshav, S., Figari, I.S., Bradley, A., and Stewart, T.A. (1993). Multiple Defects of Immune Cell Function in Mice with Disrupted Interferon-γ Genes. Science *259*, 1739–1742. https://doi.org/10.1126/science.8456300.

48. Oldenhove, G., Bouladoux, N., Wohlfert, E.A., Hall, J.A., Chou, D., Dos Santos, L.D., O'Brien, S., Blank, R., Lamb, E., Natarajan, S., et al. (2009). Decrease of Foxp3+ Treg Cell Number and Acquisition of Effector Cell Phenotype during Lethal Infection. Immunity *31*, 772–786. https://doi.org/10.1016/j.immuni.2009.10.001.

49. Sharma, M.D., Hou, D.-Y., Baban, B., Koni, P.A., He, Y., Chandler, P.R., Blazar, B.R., Mellor, A.L., and Munn, D.H. (2010). Reprogrammed Foxp3+ Regulatory T Cells Provide Essential Help to Support Cross-presentation and CD8+ T Cell Priming in Naive Mice. Immunity *33*, 942–954. https://doi.org/10.1016/j.immuni.2010.11.022.

50. Rubtsov, Y.P., Niec, R.E., Josefowicz, S., Li, L., Darce, J., Mathis, D., Benoist, C., and Rudensky, A.Y. (2010). Stability of the Regulatory T Cell Lineage in Vivo. Science *329*, 1667–1671. https://doi.org/10.1126/science.1191996.

51. Chiba, K. (2005). FTY720, a new class of immunomodulator, inhibits lymphocyte egress from secondary lymphoid tissues and thymus by agonistic activity at sphingosine 1-phosphate receptors. Pharmacol. Ther. *108*, 308–319. https://doi.org/10.1016/j.pharmthera.2005.05.002.

52. Thornton, A.M., Korty, P.E., Tran, D.Q., Wohlfert, E.A., Murray, P.E., Belkaid, Y., and Shevach, E.M. (2010). Expression of Helios, an Ikaros Transcription Factor Family Member, Differentiates Thymic-Derived from Peripherally Induced Foxp3+ T Regulatory Cells. J. Immunol. *184*, 3433–3441. https://doi.org/10.4049/jimmunol.0904028.

53. Thornton, A.M., Lu, J., Korty, P.E., Kim, Y.C., Martens, C., Sun, P.D., and Shevach, E.M. (2019). Helios+ and Helios- Treg subpopulations are phenotypically and functionally distinct and express dissimilar TCR repertoires. Eur. J. Immunol. *49*, 398–412. https://doi.org/10.1002/eji.201847935.

54. Dykema, A.G., Zhang, J., Cheung, L.S., Connor, S., Zhang, B., Zeng, Z., Cherry, C.M., Li, T., Caushi, J.X., Nishimoto, M., et al. (2023). Lung tumor–infiltrating Treg have divergent transcriptional profiles and function linked to checkpoint blockade response. Sci. Immunol. *8*, eadg1487. https://doi.org/10.1126/sciimmunol.adg1487.

55. Kanhere, A., Hertweck, A., Bhatia, U., Gökmen, M.R., Perucha, E., Jackson, I., Lord, G.M., and Jenner, R.G. (2012). T-bet and GATA3 orchestrate Th1 and Th2 differentiation through lineage-specific targeting of distal regulatory elements. Nat. Commun. *3*, 1268. https://doi.org/10.1038/ncomms2260.

56. Wei, J., Duramad, O., Perng, O.A., Reiner, S.L., Liu, Y.-J., and Qin, F.X.-F. (2007). Antagonistic nature of T helper 1/2 developmental programs in opposing peripheral induction of Foxp3+ regulatory T cells. Proc. Natl. Acad. Sci. USA *104*, 18169–18174. https://doi.org/10.1073/pnas.0703642104.

57. Hu, X., and Ivashkiv, L.B. (2009). Cross-regulation of Signaling Pathways by Interferon-γ: Implications for Immune Responses and Autoimmune Diseases. Immunity *31*, 539–550. https://doi.org/10.1016/j.immuni.2009.09.002.

58. Moriggl, R., Topham, D.J., Teglund, S., Sexl, V., McKay, C., Wang, D., Hoffmeyer, A., van van Deursen, J., Sangster, M.Y., Bunting, K.D., et al. (1999). Stat5 Is Required for IL-2-Induced Cell Cycle Progression of Peripheral T Cells. Immunity *10*, 249–259. https://doi.org/10.1016/s1074-7613(00)80025-4.

59. Afkarian, M., Sedy, J.R., Yang, J., Jacobson, N.G., Cereb, N., Yang, S.Y., Murphy, T.L., and Murphy, K.M. (2002). T-bet is a STAT1-induced regulator of IL-12R expression in naïve CD4+ T cells. Nat. Immunol. *3*, 549–557. https://doi.org/10.1038/ni794.

60. Iwata, S., Mikami, Y., Sun, H.-W., Brooks, S.R., Jankovic, D., Hirahara, K., Onodera, A., Shih, H.-Y., Kawabe, T., Jiang, K., et al. (2017). The Transcription Factor T-bet Limits Amplification of Type I IFN Transcriptome and Circuitry in T Helper 1 Cells. Immunity *46*, 983–991.e4. https://doi.org/10.1016/j.immuni.2017.05.005.

61. Garg, G., Muschaweckh, A., Moreno, H., Vasanthakumar, A., Floess, S., Lepennetier, G., Oellinger, R., Zhan, Y., Regen, T., Hiltensperger, M., et al. (2019). Blimp1 Prevents Methylation of Foxp3 and Loss of Regulatory T Cell Identity at Sites of Inflammation. Cell Rep. *26*, 1854–1868.e5. https://doi.org/10.1016/j.celrep.2019.01.070.

62. Osman, A., Yan, B., Li, Y., Pavelko, K.D., Quandt, J., Saadalla, A., Singh, M.P., Kazemian, M., Gounari, F., and Khazaie, K. (2021). TCF-1 controls Treg cell functions that regulate inflammation, CD8+ T cell cytotoxicity and severity of colon cancer. Nat. Immunol. *22*, 1152–1162. https://doi.org/10.1038/s41590-021-00987-1.

63. Daniel, V., Sadeghi, M., Wang, H., and Opelz, G. (2011). CD4+CD25+Foxp3+IFN-γ+ human induced T regulatory cells are induced by interferon-γ and suppress alloresponses nonspecifically. Hum. Immunol. *72*, 699–707. https://doi.org/10.1016/j.humimm.2011.05.020.

64. Di Pilato, M.D., Kim, E.Y., Cadilha, B.L., Prüßmann, J.N., Nasrallah, M.N., Seruggia, D., Usmani, S.M., Misale, S., Zappulli, V., Carrizosa, E., et al. (2019). Targeting the CBM complex causes Treg cells to prime tumours for immune checkpoint therapy. Nature *570*, 112–116. https://doi.org/10.1038/s41586-019-1215-2.

65. Koch, M.A., Tucker-Heard, G., Perdue, N.R., Killebrew, J.R., Urdahl, K.B., and Campbell, D.J. (2009). The transcription factor T-bet controls regulatory T cell homeostasis and function during type 1 inflammation. Nat. Immunol. *10*, 595–602. https://doi.org/10.1038/ni.1731.

66. Shankaran, V., Ikeda, H., Bruce, A.T., White, J.M., Swanson, P.E., Old, L.J., and Schreiber, R.D. (2001). IFNγ and lymphocytes prevent primary tumour development and shape tumour immunogenicity. Nature *410*, 1107–1111. https://doi.org/10.1038/35074122.

67. Kastenmüller, W., Brandes, M., Wang, Z., Herz, J., Egen, J.G., and Germain, R.N. (2013). Peripheral Prepositioning and Local CXCL9 Chemokine-Mediated Guidance Orchestrate Rapid Memory CD8+ T Cell Responses in the Lymph Node. Immunity *38*, 502–513. https://doi.org/10.1016/j.immuni.2012.11.012.

68. Moreno Ayala, M.A.M., Campbell, T.F., Zhang, C., Dahan, N., Bockman, A., Prakash, V., Feng, L., Sher, T., and DuPage, M. (2023). CXCR3 expression in regulatory T cells drives interactions with type I dendritic cells in tumors to restrict CD8+ T cell antitumor immunity. Immunity *56*, 1613–1630.e5. https://doi.org/10.1016/j.immuni.2023.06.003.

69. Spranger, S., Dai, D., Horton, B., and Gajewski, T.F. (2017). Tumor-Residing Batf3 Dendritic Cells Are Required for Effector T Cell Trafficking and Adoptive T Cell Therapy. Cancer Cell *31*, 711–723.e4. https://doi.org/10.1016/j.ccell.2017.04.003.

70. Chow, M.T., Ozga, A.J., Servis, R.L., Frederick, D.T., Lo, J.A., Fisher, D.E., Freeman, G.J., Boland, G.M., and Luster, A.D. (2019). Intratumoral Activity of the CXCR3 Chemokine System Is Required for the Efficacy of Anti-PD-1 Therapy. Immunity *50*, 1498–1512.e5. https://doi.org/10.1016/j.immuni.2019.04.010.

71. Lim, R.J., Salehi-Rad, R., Tran, L.M., Oh, M.S., Dumitras, C., Crosson, W.P., Li, R., Patel, T.S., Man, S., Yean, C.E., et al. (2024). CXCL9/10-engineered dendritic cells promote T cell activation and enhance immune

Please cite this article in press as: Maltez et al., Agonistic anti-CD40 antibody treatment converts resident regulatory T cells into activated type 1 effectors within the tumor microenvironment, Immunity (2026), https://doi.org/10.1016/j.immuni.2026.03.011

checkpoint blockade for lung cancer. Cell Rep. Med. *5*, 101479. https://doi.org/10.1016/j.xcrm.2024.101479.

72. Macian, F. (2005). NFAT proteins: key regulators of T-cell development and function. Nat. Rev. Immunol. *5*, 472–484. https://doi.org/10.1038/nri1632.
73. Marangoni, F., Zhakyp, A., Corsini, M., Geels, S.N., Carrizosa, E., Thelen, M., Mani, V., Prüßmann, J.N., Warner, R.D., Ozga, A.J., et al. (2021). Expansion of tumor-associated Treg cells upon disruption of a CTLA-4-dependent feedback loop. Cell *184*, 3998–4015.e19. https://doi.org/10.1016/j.cell.2021.05.027.
74. Pesic, M., Bartholomäus, I., Kyratsous, N.I., Heissmeyer, V., Wekerle, H., and Kawakami, N. (2013). 2-photon imaging of phagocyte-mediated T cell activation in the CNS. J. Clin. Investig. *123*, 1192–1201. https://doi.org/10.1172/jci67233.
75. Marangoni, F., Murooka, T.T., Manzo, T., Kim, E.Y., Carrizosa, E., Elpek, N.M., and Mempel, T.R. (2013). The Transcription Factor NFAT Exhibits Signal Memory during Serial T Cell Interactions with Antigen-Presenting Cells. Immunity *38*, 237–249. https://doi.org/10.1016/j.immuni.2012.09.012.
76. Radtke, A.J., Kandov, E., Lowekamp, B., Speranza, E., Chu, C.J., Gola, A., Thakur, N., Shih, R., Yao, L., Yaniv, Z.R., et al. (2020). IBEX: A versatile multiplex optical imaging approach for deep phenotyping and spatial analysis of cells in complex tissues. Proc. Natl. Acad. Sci. USA *117*, 33455–33465. https://doi.org/10.1073/pnas.2018488117.
77. Link, J.M., Eng, J.R., Pelz, C., MacPherson-Hawthorne, K., Worth, P.J., Sivagnanam, S., Keith, D., Owen, S., Langer, E.M., Grossblatt-Wait, A., et al. (2025). Ongoing replication stress tolerance and clonal T cell responses distinguish liver an dlung recurrence and outcomes in pancreatic cancer. Nature Cancer *6*, 123–144. https://doi.org/10.1038/s43018-024-00881-3.
78. Fife, B.T., Pauken, K.E., Eagar, T.N., Obu, T., Wu, J., Tang, Q., Azuma, M., Krummel, M.F., and Bluestone, J.A. (2009). Interactions between PD-1 and PD-L1 promote tolerance by blocking the TCR–induced stop signal. Nat. Immunol. *10*, 1185–1192. https://doi.org/10.1038/ni.1790.
79. Tadokoro, C.E., Shakhar, G., Shen, S., Ding, Y., Lino, A.C., Maraver, A., Lafaille, J.J., and Dustin, M.L. (2006). Regulatory T cells inhibit stable contacts between CD4+ T cells and dendritic cells in vivo. J. Exp. Med. *203*, 505–511. https://doi.org/10.1084/jem.20050783.
80. Komatsu, N., Mariotti-Ferrandiz, M.E., Wang, Y., Malissen, B., Waldmann, H., and Hori, S. (2009). Heterogeneity of natural Foxp3+ T cells: A committed regulatory T-cell lineage and an uncommitted minor population retaining plasticity. Proc. Natl. Acad. Sci. USA *106*, 1903–1908. https://doi.org/10.1073/pnas.0811556106.
81. Wei, S.C., Anang, N.A.S., Sharma, R., Andrews, M.C., Reuben, A., Levine, J.H., Cogdill, A.P., Mancuso, J.J., Wargo, J.A., Pe'er, D., et al. (2019). Combination anti-CTLA-4 plus anti-PD-1 checkpoint blockade utilizes cellular mechanisms partially distinct from monotherapies. Proc. Natl. Acad. Sci. USA *116*, 22699–22709. https://doi.org/10.1073/pnas.1821218116.
82. Hatzioannou, A., Banos, A., Sakelaropoulos, T., Fedonidis, C., Vidali, M.-S., Köhne, M., Händler, K., Boon, L., Henriques, A., Koliaraki, V., et al. (2020). An intrinsic role of IL-33 in Treg cell–mediated tumor immunoevasion. Nat. Immunol. *21*, 75–85. https://doi.org/10.1038/s41590-019-0555-2.
83. Overacre-Delgoffe, A.E., Chikina, M., Dadey, R.E., Yano, H., Brunazzi, E.A., Shayan, G., Horne, W., Moskovitz, J.M., Kolls, J.K., Sander, C., et al. (2017). Interferon-γ Drives Treg Fragility to Promote Anti-tumor Immunity. Cell *169*, 1130–1141.e11. https://doi.org/10.1016/j.cell.2017.05.005.
84. Liudahl, S.M., Betts, C.B., Sivagnanam, S., Morales-Oyarvide, V., da da Silva, A., Yuan, C., Hwang, S., Grossblatt-Wait, A., Leis, K.R., Larson, W., et al. (2021). Leukocyte Heterogeneity in Pancreatic Ductal Adenocarcinoma: Phenotypic and Spatial Features Associated with Clinical Outcome. Cancer Discov. *11*, 2014–2031. https://doi.org/10.1158/2159-8290.cd-20-0841.
85. Carpenter, A.E., Jones, T.R., Lamprecht, M.R., Clarke, C., Kang, I.H., Friman, O., Guertin, D.A., Chang, J.H., Lindquist, R.A., Moffat, J., et al. (2006). CellProfiler: image analysis software for identifying and quantifying cell phenotypes. Genome Biol. *7*, R100. https://doi.org/10.1186/gb-2006-7-10-r100.
86. Kawabe, T., Naka, T., Yoshida, K., Tanaka, T., Fujiwara, H., Suematsu, S., Yoshida, N., Kishimoto, T., and Kikutani, H. (1994). The immune responses in CD40-deficient mice: Impaired immunoglobulin class switching and germinal center formation. Immunity *1*, 167–178. https://doi.org/10.1016/1074-7613(94)90095-7.
87. Huang, S., Hendriks, W., Althage, A., Hemmi, S., Bluethmann, H., Kamijo, R., Vilček, J., Zinkernagel, R.M., and Aguet, M. (1993). Immune Response in Mice that Lack the Interferon-γ Receptor. Science *259*, 1742–1745. https://doi.org/10.1126/science.8456301.
88. Jung, S., Unutmaz, D., Wong, P., Sano, G.-I., los De los Santos, K.D., Sparwasser, T., Wu, S., Vuthoori, S., Ko, K., Zavala, F., et al. (2002). In Vivo Depletion of CD11c+ Dendritic Cells Abrogates Priming of CD8+ T Cells by Exogenous Cell-Associated Antigens. Immunity *17*, 211–220. https://doi.org/10.1016/s1074-7613(02)00365-5.
89. Richman, L.P., and Vonderheide, R.H. (2014). Role of Crosslinking for Agonistic CD40 Monoclonal Antibodies as Immune Therapy of Cancer. Cancer Immunol. Res. *2*, 19–26. https://doi.org/10.1158/2326-6066.cir-13-0152.
90. Winograd, R., Byrne, K.T., Evans, R.A., Odorizzi, P.M., Meyer, A.R.L., Bajor, D.L., Clendenin, C., Stanger, B.Z., Furth, E.E., Wherry, E.J., et al. (2015). Induction of T-cell Immunity Overcomes Complete Resistance to PD-1 and CTLA-4 Blockade and Improves Survival in Pancreatic Carcinoma. Cancer Immunol. Res. *3*, 399–411. https://doi.org/10.1158/2326-6066.cir-14-0215.
91. Hay, C.A., Sor, R., Flowers, A.J., Clendenin, C., and Byrne, K.T. (2019). Ultrasound-Guided Orthotopic Implantation of Murine Pancreatic Ductal Adenocarcinoma. J. Vis. Exp. https://doi.org/10.3791/60497.
92. Vonderheide, R.H. (2019). CD40 Agonist Antibodies in Cancer Immunotherapy. Annu. Rev. Med. *71*, 47–58. https://doi.org/10.1146/annurev-med-062518-045435.

Please cite this article in press as: Maltez et al., Agonistic anti-CD40 antibody treatment converts resident regulatory T cells into activated type 1 effectors within the tumor microenvironment, Immunity (2026), https://doi.org/10.1016/j.immuni.2026.03.011

STAR★METHODS

KEY RESOURCES TABLE

REAGENT or RESOURCE	SOURCE	IDENTIFIER
Antibodies		
InVivoMAb anti-mouse aCD40	BioXCell	Cat # BE0016-2; RRID: AB_1107647
InVivoMAb rat IgG2a isotype control, anti-trinitrophenol	BioXCell	Cat # BE0089; RRID: AB_1107769
InVivoMAb anti-mouse PD-1	BioXCell	Cat # BE0146; RRID: AB_10949053
InVivoMAb anti-mouse CTLA-4	BioXCell	Cat # BE0131; RRID: AB_10950185
InVivoMAb anti-mouse MHC Class II	BioXCell	Cat # BE0108; RRID: AB_10949298
InVivoMAb anti-mouse IL-12p40	BioXCell	Cat # BE0051; RRID: AB_1107698
InVivoMAb anti-mouse IFN-gamma	BioXCell	Cat # BE0055; RRID: AB_1107694
InVivoPlus anti-mouse polyclonal Syrian hamster IgG	BioXCell	Cat #BP0087; RRID: AB_1107782
CD45 Alexa Fluor 700	Biolegend	Cat # 103128; RRID: AB_493715
CD25 PE	Biolegend	Cat # 102008; RRID: AB_312857
CD3ε PE/Cyanine5	Biolegend	Cat # 100274; RRID: AB_2894410
CD8a BV711	Biolegend	Cat # 563046; RRID: AB_273792
CD8a PE-CF594	BD Biosciences	Cat # 562283; RRID: AB_11152075
CD4 BUV805	BD Biosciences	Cat # 612900; RRID: AB_2827960
CD4 Brilliant Violet 785	Biolegend	Cat # 100552;RRID: AB_2563053
Foxp3 Brilliant Violet 421	Biolegend	Cat # 126419: RRID: AB_2565933
Foxp3 PE	Biolegend	Cat # 126404: RRID: AB_1089117
Foxp3 PE-Cyanine7	Thermo Fisher Scientific	Cat # 25-5773-82; RRID: AB_891552
Tbet Brilliant Violet 785	Biolegend	Cat # 644835: RRID: AB_2721566
TCF1 PE	Biolegend	Cat # 655208: RRID: AB_2728492
Blimp1 APC	Biolegend	Cat # 150008; RRID: AB_2728187
CD44 BUV395	BD Biosciences	Cat # 740215: RRID: AB_2739963
IFN gamma PE-Cyanine7	Thermo Fisher Scientific	Cat # 25-7311-82; RRID: AB_469680
CD3 AF532	Invitrogen	Cat # 58-0032-82; RRID: AB_11217479
CD3 AF594	Biolegend	Cat # 100240; RRID: AB_2563427
CD4 AF488	Biolegend	Cat # 100529: RRID: AB_389303
CD8a AF594	Biolegend	Cat # 100758: RRID: AB_2563237
CD8a eF450	Thermo Fisher Scientific	Cat # 48-0081-80; RRID: AB_1272235
Foxp3 eF660	Invitrogen	Cat # 50-5773-82; RRID: AB_11218868
CD11b AF488	Biolegend	Cat # 101217; RRID: AB_389305
CD11c AF647	Biolegend	Cat # 117312; RRID: AB_389328
Helios APC	Invitrogen	Cat # 17-9883-42; RRID: AB_2573322
CD103 unconjugated	R&D Systems	Cat # AF1990; RRID: AB_2128618
MHC-II AF700	Biolegend	Cat # 107622; RRID: AB_493727
NFAT1 unconjugated	Cell Signaling Technology	Cat # 5861; RRID: AB_10834808
NFAT1 AF647	Cell Signaling Technology	Cat # 14201; RRID: AB_2798423
pSTAT5 unconjugated	Cell Signaling Technology	Cat # 9359; RRID: AB_823649
pSTAT1 unconjugated	Cell Signaling Technology	Cat # 9167; RRID: AB_561294
Goat anti-Rabbit IgG AF594	Invitrogen	Cat # A11037; RRID: AB_2534095
Donkey anti-Goat IgG AF594	Invitrogen	Cat # A32758; RRID: AB_2762828
Donkey anti-Rabbit IgG Dylight 488	Biolegend	Cat # 406404; RRID: AB_1575130
anti-human TBET	Cell Signalling Technologies	Cat # 13232S; RRID: AB_2616022
anti-human CD3	Thermo Fisher Scientific	Cat # RM-9107-S; RRID: AB_149924
anti-human CD8	Thermo Fisher Scientific	Cat # MA5-13473; RRID: AB_11000353

(*Continued on next page*)

Please cite this article in press as: Maltez et al., Agonistic anti-CD40 antibody treatment converts resident regulatory T cells into activated type 1 effectors within the tumor microenvironment, Immunity (2026), https://doi.org/10.1016/j.immuni.2026.03.011

Continued

REAGENT or RESOURCE	SOURCE	IDENTIFIER
anti-human Foxp3	eBioscience	Cat # 14-4777-82: RRID: AB_3666277
anti-human CD45	eBioscience	Cat # 14-0459-82; RRID: AB_467274
anti-HLA-DR/DP/DQ	LS Bio	Cat # LS-B10162; RRID: AB_3741033
anti-human CD3	Thermo Fsher Scientific	Cat # RM-9107-S: RRID: AB_149924
anti-human Foxp3	eBioscience	Cat # 14-4777-82; RRID: AB_467556
anti-human CD68	Abcam	Cat # ab783; RRID: AB_306119
anti-human CD11C	Abcam	Cat # ab52632; RRID: AB_212979
anti-human CD20	Abcam	Cat # ab9475; RRID: AB_570429
Biological samples		
Naïve patient tumor samples	Liudahl et al.[84]	N/A
Neoadjuvant CD40-treated patient tumor samples	Byrne et al.[15] and Blise et al.[14]	N/A
Chemicals, peptides, and recombinant proteins		
CellXVivo	R&D	Cat # CDK018
GolgiStop (Monensin)	BD Biosciences	Cat # 555029
GolgiPlug (Brefeldin A)	BD Biosciences	Cat # 554724
PMA	Sigma-Aldrich	Cat # P8139
Ionomycin	Sigma-Aldrich	Cat # I0634
Live/Dead Fixable Aqua Dead Cell Stain Kit	Thermo Fisher Scientific	Cat # L34957
Tamoxifen	Sigma-Aldrich	Cat # 10540-29-1
Sphingosine-1 phosphate agonist (FTY720)	Sigma-Aldrich	Cat # SML0700
Cytofix/Cytoperm	BD Biosciences	Cat # 554722
Lithium Borohydride	STREM chemicals	Cat # 93-0397
Xylenes (Certified ACS)	Fisher Scientific	Cat # X5-4
Concentrated (10X) Antigen Retrieval Citra Plus Solution	Fisher Scientific	Cat # NC9755543
Hematoxylin Counterstain	Vector Laboratories	Cat # H-3401-500
Eosin	Epredia	Cat # 71204
Peroxidase and Alkaline Phosphatase Blocking Reagent	Agilent Technologies	Cat # S200389-2
Histofine Simple Stain Human MAX PO (R) (for Rabbit primary antibody)	Nacalal USA	Cat # 414144F
Histofine Simple Stain Human MAX PO (M) (for Mouse primary antibody)	Nacalal USA	Cat # 414134F
ImmPACT® AEC Substrate Kit, Peroxidase, Vector laboratories, SK SK4205	Fisher Scientific	Cat # NC99451169
Sodium azide	Fisher Scientific	N/A
Animal Free Blocker and Diluent	Vector Labs	Cat # SP-5035-100
Critical commercial assays		
ACD RNAscope HiPlex12 Reagents Kit	ACD Biotechne	Cat # 324440
Experimental models: Cell lines		
$Kras^{LSL\text{-}G12D/+}$; $Trp53^{LSL\text{-}R172H/+}$; Pdx1-Cre; $Rosa26^{YFP/YFP}$ 2838c3 clonal tumor cell line	Li et al.[11] (commer cially available from Kerafast)	Cat # EUP013-FP: RRID: CVCL_YM18
B16-F10	ATCC	Cat # CRL-6475: RRID: CVC:_0159
MC38 murine colon adenocarcinoma	Eil laboratory, Kerafast	Cat # CRL-2640; RRID: CVCL_B288
MC38 OVA murine colon adenocarcinoma	Vitro Biotech	Cat # VOA 1B009
Experimental models: Organisms/strains		
C57BL/6	Jackson Laboratories	Cat # 00664; RRID: IMSR_JAX:000664
Batf3$^{-/-}$ (B6.129S(C)-*Batf3*^{tm1Kmm}/J)	Jackson Laboratories	Cat # 013755; RRID: IMSR_JAX:013755
CD40$^{-/-}$	Jackson Laboratories	Cat # 002928: RRID: IMSR_JAX:002928
IFN-gamma$^{-/-}$	Jackson Laboratories	Cat # 002287; RRID: IMSR_JAX:002287
IFN-gamma receptor$^{-/-}$	Jackson Laboratories	Cat # 003288; RRID: IMSR_JAX:003288

(*Continued on next page*)

Please cite this article in press as: Maltez et al., Agonistic anti-CD40 antibody treatment converts resident regulatory T cells into activated type 1 effectors within the tumor microenvironment, Immunity (2026), https://doi.org/10.1016/j.immuni.2026.03.011

Continued

REAGENT or RESOURCE	SOURCE	IDENTIFIER
IL-12p40$^{-/-}$	Jackson Laboratories	Cat # 002693; RRID: IMSR_JAX:002693
CD11c-DTR	Jackson Laboratories	Cat # 004509: RRID: IMSR_JAX:004509
Foxp3CreERT2 (Foxp3$^{tm9(EGFP/cre/ERT2)Ayr}$/J)	Jackson Laboratories	Cat # 016961; RRID: IMSR_JAX:016961
C57BL/6J-*Rag1*^{em10Lutzy}/*J*	Jackson Laboratories	Cat # 034159; RRID: IMSR_JAX:034159
RCL-tdTomato (B6.Cg-*Gt(ROSA) 26Sor*$^{tm9(CAG-tdTomato)Hze}$/J	Jackson Laboratories	Cat # 007909; RRID: IMSR_JAX:007909
OT-II:Rag1 [$^{-/-}$]	Taconic	Cat # 4234; RRID: IMSR_TCA:4234
Tbet-ZsGreen[Tg] Tg(Rorc-E2-Crimson)Tg(Foxp3-RFP)	Taconic	Cat # 008509
Oligonucleotides		
Probes for RNAScope:		N/A
Cd3e (Alexa Fluor 488)	ACD biotechne	Cat # 314721-T1
tdTomato (ATTO 550)	ACD biotechne	Cat # 317041-T2
Foxp3 (ATTO 647N)	ACD biotechne	Cat # 432611-T3
Ifng (Alexa Fluor 750)	ACD biotechne	Cat # 311391-T4
Cd40 (Alexa Fluor 488)	ACD biotechne	Cat # 404671-T5
Xcr1 (ATTO 550)	ACD biotechne	Cat # 562371-T6
Il12a (ATTO 647N)	ACD biotechne	Cat # 414881-T7
Itgae (Alexa Fluor 750)	ACD biotechne	Cat # 463161-T8
Cd4 (Alexa Fluor 488)	ACD biotechne	Cat # 406841-T9
Cxcl9 (ATTO 550)	ACD biotechne	Cat # 489341-T10
Cxcr3 (ATTO 647N)	ACD biotechne	Cat # 402511-T11
Software and algorithms		
BD FACSDiva	BD Biosciences	RRID: SCR_001456
FlowJo Software	Treestar	RRID: SCR_008520
Matlab Computer Vision Toolbox	The Mathworks, Inc	RRID: SCR_017581
Imaris	Oxford Instruments	Imaris software; RRID: SCR_007370
Simple ITK software	Radtke et al.[76]	Z Channel Alignment tools; RRID: SCR_024693
ImageJ	Liudahl et al.[84]	RRID: SCR_003070
Cell Profiler	Carpenter et al.[85]	RRID: SCR_007358
FCS Express Image Cytometry RUO	De Novo Software	RRID: SCR_016431
Graphpad Prism	Graphpad	RRID: SCR_002798
Other		
Beckman Coulter Counter Z2	Beckman Coulter	
LSR II	BD Biosciences	RRID: SCR_022376
Fortessa	BD Biosciences	RRID: SCR_022376; RRID: SCR_009974
Leica cryostat	Leica	RRID: SCR_020221
Leica SP8X upright microscope	Leica	
PELCO BioWave microwave	Ted Pella	Pro-36500-230; RRID: SCR_018609
PELCO SteadyTemp thermoelectric recirculating chiller	Ted Pella	Cat # Pro-50062; RRID: SCR_003070
Superfrost Plus microscopy slides	VWR	Cat # 48311-703
ACD HybEZ II Oven	ACD Biotechne	Cat # 321710
ACD EZ-Batch Slide Holder	ACD Biotechne	Cat # 321716
ACD Humidity Control Tray	ACD Biotechne	Cat # 310012
No. 1.5 coverglass	VWR	Cat # 48393-241
Optimal Cutting Temperature (O.C.T.)	Sakura Finetek	Cat # 50-363-579
Fluoromount-G	SouthernBiotech	Cat # 0100-01; RRID: SCR_015961
Surgipath DB80LX blade	Leica	Cat # 14035843497
CD4 T cell isolation kit	MACS Miltenyi	Cat # 130-104-453

Please cite this article in press as: Maltez et al., Agonistic anti-CD40 antibody treatment converts resident regulatory T cells into activated type 1 effectors within the tumor microenvironment, Immunity (2026), https://doi.org/10.1016/j.immuni.2026.03.011

CellPress

Mice

Mice were bred and maintained under specific pathogen-free conditions at an American Association for the Accreditation of Laboratory Animal Care (AAALAC)-accredited animal facilities within the NIAID, the University of Pennsylvania, or Oregon Health and Science University. Mice were housed in accordance with the procedures outlined in the NIH Guide for the Care and Use of Laboratory Animals (NIAID Protocol # LISB-4E), or in compliance with the procedures that were reviewed and approved by the Institutional Animal Care and Use Committee of the University of Pennsylvania (Protocol # 804666) or Oregon Health and Science University (Protocol # 4153). Unless otherwise stated, sex and age-matched littermates (6–12 weeks of age, both sexes) were used for individual experiments. The following strains were purchased from Jackson Laboratories (Bar Harbor, ME): C57BL/6 (Cat # 00664), *Batf3*$^{-/-}$ (B6.129S(C)-*Batf3*^{tm1Kmm}/J) (Cat # 013755),[43] CD40$^{-/-}$ (Cat # 002928),[86] IFN-$\gamma^{-/-}$ (Cat # 002287),[47] IFN-γR$^{-/-}$ (Cat # 003288),[87] IL-12p40$^{-/-}$ (Cat # 002693),[46] CD11c-DTR (Cat # 004509),[88] Foxp3CreERT2 (Foxp3$^{tm9(EGFP/cre/ERT2)Ayr}$/J) (Cat # 016961),[50] C57BL/6J-*Rag1*^{em10Lutzy}/J (Cat # 034159), RCL-tdTomato (B6.Cg-*Gt(ROSA)26Sor*$^{tm9(CAG-tdTomato)Hze}$/J (Cat # 007909).[46] C57BL/6J.Ly5a mice were purchased from the NIAID-Taconic exchange platform: OT-II:Rag1 [$^{-/-}$] (Taconic Cat # 4234), Tbet-ZsGreen[Tg] Tg(Rorc-E2-Crimson)Tg(Foxp3-RFP) (Taconic Cat # 008509) and referenced as Tbet/Foxp3 reporter mice in the text. Foxp3CreERT2 (Foxp3$^{tm9(EGFP/cre/ERT2)Ayr}$/J) and RCL-tdTomato (B6.Cg-*Gt(ROSA)26Sor*$^{tm9(CAG-tdTomato)Hze}$/J were crossed at both the NIAID and University of Pennsylvania facilities and only male F1 offspring ('Foxp3 Lineage mice') were used in experiments.

METHOD DETAILS

In vivo reagents and treatments

Mice were treated with αCD40/αPD-1/αCTLA-4 ('FPC') as previously described.[13] Briefly, αPD-1 (RMP1-14; BioXcell, Cat # BE0146; 200 μg/dose) was injected intraperitoneally (i.p.) on days 0, 3, 6, 9, 12, 15 and αCTLA-4 (9H10; BioXcell, Cat # BE0131; 200 μg/dose) on days 0, 3, and 6, with a single dose of agonistic αCD40 (FGK4.5; BioXcell, Cat # BE0016-2; 100 μg) on day 3.[13] Clone FGK4.5 is a potent agonist for CD40 as previously described.[89] For isotype controls, rat IgG2a (2A3; BioXcell, Cat # BE0089; 100 -300 μg, depending on the treatment cohort) was used. All antibodies were endotoxin free. Note that although αCTLA-4 clone 9H10 has previously been reported to deplete Treg cells, we have previously reported that Treg cell depletion is lessened in the PDAC TME as compared to B16 melanoma.[13] We have previously reported that we observed no toxicities with this treatment regimen.[13,90] For clarification, FPC treated mice received αPD-1, αCTLA-4, and αCD40. PC treated mice received αPD-1/αCTLA-4 and isotype control for αCD40, while Control treated mice received only isotype controls, and neither PC nor FPC.

For MHC-II blockade, mice were i.p. injected with a single 1.0 mg/kg dose of αMHC-II (M5/114; BioXcell, Cat # BE0108) 12 hours prior to agonistic αCD40 administration. Mice were harvested 24 hours after αCD40 (day 4 post therapy start). For isotype controls, rat IgG2a (2A3; BioXcell; 200 μg) was used. All antibodies were endotoxin free.

For IL-12p40 and IFN-γ blockades, mice were injected i.p. with 200 μg/dose of αIL12p40 (C17.8, BioXcell, Cat # BE0051) or αIFN-γ (XMG1.2, BioXcell, Cat # BE0055) one day prior to starting therapy, 12 hours before agonistic αCD40, and 24 hours after agonistic αCD40 (days -1, 2.5, and 4). For isotype controls, rat IgG2a (2A3; BioXcell; 200 μg) was used. Mice were harvested 48 hours after agonistic αCD40 (day 5 post therapy start). All antibodies were endotoxin free.

Tamoxifen (Sigma-Aldrich, Cat # 10540-29-1) was dissolved in corn oil at a concentration of 20 mg/ml and male Foxp3CreERT2^{+}–R26tdTomato$^{+/-}$ animals received 100 μl of tamoxifen emulsion (75 mg tamoxifen/kg) or corn oil control administered intraperitoneally daily on days 6-8 post tumor implantation.[50] Animals were then treated with isotype or monoclonal antibody therapies as described above. Diphtheria toxin (DT) was administered at 8ng/g every 48hours for CD11c-DT receptor mice[88] starting 24 hours before CD40 agonist treatment.

For lymphocyte trafficking blockade, mice were injected i.p. with 20 μg of FTY720 (Sigma-Aldrich, Cat # SML0700) daily starting at the time of initial αPD-1/αCTLA-4 treatment through experimental endpoint (five days later).

Implantation of tumor cell clones

Kras$^{LSL-G12D/+}$; Trp53$^{LSL-R172H/+}$; Pdx1-Cre; Rosa26$^{YFP/YFP}$ 2838c3 tumor cells were generated from a female mouse and used as previously described,[11] and are also commercially available (Kerafast). B16-F10 and MC38 were purchased from ATCC. Cells were cultured in DMEM (high glucose without sodium pyruvate) with 10% FBS (Gibco) and glutamine (2.0 mM) and harvested when confluent. Cells were dissociated into single cells with 0.25% trypsin (Gibco), washed with serum-free Dulbecco's Modified Eagle's medium (DMEM) twice, and counted in preparation for subcutaneous implantation. 2.5x10^5 PDAC tumor cells, or 1.5x10^5 B16-F10 melanoma cells, or 3x10^5 MC38 cells were implanted subcutaneously, or 5x10^6 PDAC cells were implanted orthotopically into the pancreas,[91] with viability >90% for each experiment. This cell line was examined by the Infectious Microbe PCR Amplification Test (IMPACT) and authenticated to be free of contamination by the Research Animal Diagnostic Laboratory (RADIL) at the University of Missouri.

OT-II and MC38

Mice were subcutaneously injected with 5x10^5 MC38 (WT) in the left flank and 5x10^5 MC38-OVA (ovalbumin) in the right flank. Nine days post tumor implantation differentiated OT-II cells were transferred intravenously. In brief, naïve CD4$^+$ T cells were isolated from OVA-specific CD4$^+$ T cell receptor transgenic (OT-II) mouse spleens using the MACS kit from Miltenyi (Cat # 130-104-453). Cells were then differentiated ex vivo (R&D, CellXVivo, Cat # CDK018) for 3 days and 1.5 million cells were transferred into tumor-bearing Rag1 $^{-/-}$ recipient mice. Tumors were harvested 3 days post OT-II transfer and imaged for NFAT1 nuclear translocation.

Please cite this article in press as: Maltez et al., Agonistic anti-CD40 antibody treatment converts resident regulatory T cells into activated type 1 effectors within the tumor microenvironment, Immunity (2026), https://doi.org/10.1016/j.immuni.2026.03.011

Subcutaneous tumor growth, regression, and animal survival assessment

Tumor sizes were measured every 2–3 days for tumor growth assessment experiments. Tumor length and width were measured with calipers and tumor volumes were then calculated as length*width^2/2. Tumor volumes of 500 mm^3 were used as an endpoint for survival analysis. Tumor regressions and waterfall plots were calculated using the initial tumor size at the start of treatment to tumor size 21 days later.

Tissue section preparation, processing, and immunostaining

At indicated time points, mice were euthanized and tumors were quickly harvested and fixed for 14-16 hr. at 4°C in BD Cytosis/Cytoperm (BD Bioscience, Cat # 554722) diluted 1:4 in PBS. Tumors were washed 3x in PBS (5 min per wash), carefully trimmed of fat using a stereo dissection microscope and fine forceps and dehydrated for 24 hr. in a 30% sucrose solution made in 0.1 M PBS. Tumors were then embedded in optimal cutting temperature (O.C.T.) compound (Sakura Finetek, Cat # 50-363-579), frozen on dry ice, and stored at –80°C. 18-50 μm tumor sections were prepared using a cryostat (Leica) equipped with a Surgipath DB80LX blade (Leica, Cat # 14035843497). Cryochamber and specimen cooling was set to –17°C.

Tissue sections were adhered to Superfrost Plus microscopy slides (VWR, Cat #: 48311-703), blocked and permeabilized using 0.3% Triton X-100 and 1:50 with Fc block (CD16/CD32, clone 2.4G2, BD Biosciences, Cat # 553141) for 1 hr. at room temperature (22°C), and washed in PBS. Tissue sections were next incubated with directly conjugated antibodies diluted in PBS for either 15 hr. at 4°C or using a PELCO BioWave Pro-36500-230 microwave in conjunction with a PELCO SteadyTemp Pro-50062 thermoelectric recirculating chiller (Ted Pella). Briefly, a 2-1-2-1-2-1-2-1-2 program was used for immunolabeling, where "2" denotes 2 min at 100 W and "1" denotes 1 min at 0 W. This program was run twice for primary antibody labeling and once for secondary antibody labeling as previously described.[76] After washing 3x in PBS (5 min per wash) at 22°C, samples were mounted in Fluoromount-G (SouthernBiotech, Cat # 0100-01), which was allowed to cure for a minimum of 14 hrs at 22°C. All imaging was performed using No. 1.5 coverglass (VWR, Cat # 48393-241).

IBEX

After all the steps outlined in the previous section, slides/tissues were run through our IBEX protocol. In brief, slides were submerged in PBS to facilitate coverslip removal for a minimum of 1 hr. at 22°C. Upon cover slip removal, tissue sections were fluorophore bleached using 1.0 mg/ml solution of lithium borohydride for 15 minutes. Slides were washed 3x in PBS and then re-stained as described above. Images across the two cycles were aligned using Simple iTK algorithms as described.[76]

Antibodies for Immunofluorescence

All antibodies were used at a dilution of 1:50 and have been previously validated for IF and IBEX within our laboratory[76] with the exception of nuclear NFAT1 (Figure S7). Treg cell identification always included a Foxp3 detection antibody. Combinations of the following antibodies were used for immunostaining: Hoescht; CD3 (17A2; AF532, Invitrogen, Cat # 58-0032-82); CD3 (17A2; AF594, BioLegend, Cat # 100240); CD4 (RM4-5; AF488, BioLegend, Cat # 100529); CD8a (53-6.7; AF594, BioLegend, Cat # 100758); CD8a (53-6.7; eF450, ThermoFisher, Cat # 48-0081-80); Foxp3 (FJK-16s; eF660, Invitrogen, Cat # 50-5773-82); CD11b (M1/70; AF488, BioLegend, Cat # 101217); CD11c (N418; AF647, BioLegend, Cat # 117312); CD103 (Itgae; unconjugated, R&D Systems, Cat # AF1990); MHC-II (M5/114.152; AF700, BioLegend, Cat # 107622); NFAT1 (D43B1; unconjugated, CST, Cat # 5861S); NFAT1 (D43B1; AF647, CST, Cat # 14201S); pSTAT1 (58D6; unconjugated, CST, Cat # 9167L); Helios (22F6; APC, Invitrogen, Cat # 17-9883-42); Cleaved caspase-3 (Asp175/D3E9; unconjugated, CST, Cat # 9579S); Donkey anti-Goat IgG (H+L; AF594, Invitrogen, Cat # A32758); Donkey anti-Rabbit IgG (H+L; Dylight 488, BioLegend, Cat # 406404); Goat anti-Rabbit IgG (H+L; AF594, Invitrogen, Cat # A11037).

RNAScope

Tissues were prepared and stained following the ACD biotechne user manual for RNAscope HiPlex Assay (Document # 324100-UM, Chapters 3-4, Fresh Frozen). Briefly, tumors were harvested and immediately placed into OCT and frozen fresh on dry ice. Tissue sections were cut as described above. Slides were stored until use at -80 °C, then immediately fixed in 4% PFA for 1 hour at 22°C. Slides were dehydrated in sequential ethanol steps (50%, 70%, 100%) and were then ready for staining using the ACD EZ-Batch Slide Holder (Cat # 321716), Humidity Control Tray (Cat # 310012), and HybEZ II Oven (Cat # 321710) system. HiPlex probes (supplied at 50X concentration) were used iteratively for (cycle 1) *Cd3e* (Cat # 314721-T1, Alexa Fluor 488), *tdTomato* (Cat # 317041-T2, ATTO 550), *Foxp3* (Cat # 432611-T3, ATTO 647N), and *Ifng* (Cat # 311391-T4, Alexa Fluor 750); (cycle 2) *Cd40* (Cat # 404671-T5, Alexa Fluor 488), *Xcr1* (Cat # 562371-T6, ATTO 550), *Il12a* (Cat # 414881-T7, ATTO 647N), and *Itgae* (Cat # 463161-T8, Alexa Fluor 750); (cycle 3) *Cd4* (Cat # 406841-T9, Alexa Fluor 488), *Cxcl9* (Cat # 489341-T10, ATTO 550), and *Cxcr3* (Cat # 402511-T11, ATTO 647N). Probes were hybridized for 2 hours in the oven at 40 °C. Slides were then washed, and the probes sequentially amplified using the HiPlex8 Detection Kit (Cat # 324110). Samples were counterstained with DAPI and mounted in Fluoromount-G (SouthernBiotech, Cat # 0100-01). All imaging was performed using No. 1.5 coverglass (VWR, Cat # 48393-241).

Laser scanning confocal microscopy

Images were acquired using an upright Leica TCS SP8 X spectral detection system (Leica) equipped with a pulsed white light laser, 4 Gallium-Arsenide Phosphide (GaAsP) Hybrid Detectors (HyDs), 1 photomultiplier tube (PMT), 40x (NA = 1.3) or 20x (NA = 0.75) oil

Please cite this article in press as: Maltez et al., Agonistic anti-CD40 antibody treatment converts resident regulatory T cells into activated type 1 effectors within the tumor microenvironment, Immunity (2026), https://doi.org/10.1016/j.immuni.2026.03.011

immersion objective lenses, and a motorized stage. For tissue sections (18-50 μm), images were acquired using the 20x objection with 1.5 zoom, z step size of 0.5-1.5 μm, and detector bit-depth of 12. RNAscope images were acquired using an inverted Leica Stellaris, which is optimized for far-red laser excitation and emission detection above 700 nm. In all experiments, image acquisition was controlled using LAS X software.

Image processing, segmentation, and analysis

Image files generated in LAS X software were converted into ''.ims'' files in Imaris software (Bitplane) and subjected to a 1-pixel Gaussian filter to reduce noise. Image segmentation was performed in Imaris using the ''Surface Object Creation'' module, which employs a seeded region growing, k-means, and watershed algorithm to define individual cells. Segmentation artifacts were excluded using a combination of sphericity and volume thresholds, as well as manual correction. Following cell segmentation and surface creation, the mean or summed voxel fluorescence intensity values per channel were assessed in Imaris. In certain instances, these fluorescence distributions were used to selectively visualize T cells with specific phenotypes by creating discrete thresholds using the ''filter'' tool. For spatial statistics, the ''shortest distance to object'' function was used in Imaris which can automatically calculate the distance between two objects (such as shortest distance from a defined Treg cell to the tumor edge).

Imaris algorithm for Foxp3 Lineage tumor analyses

[Algorithm]
Enable Region Of Interest = true
Process Entire Image = true
Enable Region Growing = true
Enable Tracking = false
Enable Classify = false
Enable Shortest Distance = false
[Region of Interest]
Region1: XYZT from [12973 8840 1 1] to [15020 10906 1 1]
[Segmentation Setup]
Source Channel Index = 2
Enable Smooth = true
Surface Grain Size = 1.50 μm
Enable Eliminate Background = true
Diameter Of Largest Sphere = 4.50 μm
[Threshold]
Active Threshold = true
Enable Automatic Threshold = false
Manual Threshold Value = 1.11121
Active Threshold B = false
Region Growing Estimated Diameter = 5.50 μm
Region Growing Morphological Split = false
[Filter Seed Points]
"Quality" above 2.29
[Filter Surfaces]
"Number of Voxels Img=1" above 10.0

Flow cytometry of murine tumor samples

At the indicated time points after αCD40 administration (equivalent to day five after the start of FPC treatment), mice were sacrificed and tumors prepared for single cell suspension as previously described.[13] Briefly, tumors were washed with PBS, then minced and incubated for 45 minutes in 1mg/mL collagenase XI with protease inhibitor at 37°C and filtered through a 70 μM cell strainer with cold PBS supplemented with 0.5% BSA and 2mM ethylenediaminetetraacetic acid (EDTA). Cells were counted with Beckman Coulter Counter Z2 (Beckman Coulter) and stained with Live/Dead Fixable Aqua Dead Cell Stain Kit (Thermo Fisher Scientific, Cat # L34957). Cell surface molecules were assessed by incubating single cell suspensions from tissues with primary fluorophore-conjugated antibodies on ice for 45 minutes in PBS with 0.5% bovine serum albumin and 2.0 mM EDTA. For intracellular cytokine quantification, single cell suspensions were incubated for 4hours at 37°C with PMA (Sigma-Aldrich, Cat # P8139) with ionomycin (Sigma-Aldrich, Cat # I0634) and incubated with GolgiPlug (Brefeldin A) and GolgiStop (Monensin) (BD Biosciences, Cat # 555029 and 554724, respectively). Intracellular staining was performed using the CytoFix/Cytoperm kit (BD Bioscience, Cat # 554722) according to the manufacturer's instructions. Combinations of the following antibodies were used at 1:100 for flow cytometric analysis: Foxp3 (clone MF-14, BV421, Biolegend, Cat # 126419 or PE, Biolegend, Cat # 126404; or clone FJK-16s, PECy7, eBioscience, Cat # 25-5773-82), CD44 (clone IM7, BUV395, BD Biosciences, Cat # 740215), Tbet (clone 4B10, BV785, Biolegend, Cat # 644835), CD8 (clone 53-6.7, BV711, BD Biosciences, Cat # 563046 or PE-CF594, BD Biosciences, Cat # 562283), CD4 (clone GK1.5, BUV805, BD Biosciences, Cat # 612900; or clone RM4-6, BV785, Biolegend, Cat # 100552), CD3e (clone 145-2C11, PE-Cy5, Biolegend, Cat #

Please cite this article in press as: Maltez et al., Agonistic anti-CD40 antibody treatment converts resident regulatory T cells into activated type 1 effectors within the tumor microenvironment, Immunity (2026), https://doi.org/10.1016/j.immuni.2026.03.011

100310), IFN-γ (clone XMG1.2, PE-Cy7, eBioscience, Cat # 25-7311-82), CD45 (clone 30-F11, AF700, Biolegend, Cat # 103128), CD25 (clone PC61, PE, Biolegend, Cat # 102008), TCF1 (clone 7F11A10, PE, Biolegend, Cat # 655208), and Blimp1 (clone 5E7, APC, Biolegend, Cat # 150008). Flow cytometric analysis was performed on an LSR II or Fortessa flow cytometer (BD Biosciences) using BD FACSDiva software and analyzed using FlowJo software (Treestar).

Multiplexed immunohistochemistry (mIHC) analysis of patient samples

Tumor samples were obtained with informed consent in accordance with the Declaration of Helsinki and treatment-naïve patient samples were acquired from the Oregon Pancreas Tissue Registry under Oregon Health and Science University IRB protocol #3609,[84] while neoadjuvant αCD40-treated patient samples were acquired from an open-label, Phase I clinical trial (Cancer Immunotherapy Trials Network CITN11-01; NCT02588443).[14,15] Patients received selicrelumab, an agonistic CD40 IgG2 antibody with high potency.[92] Formalin-fixed, paraffin-embedded (FFPE) surgical tissue samples were sectioned and assessed using hematoxylin and eosin (H&E), as well as chromagen-based mIHC. Using pathologist annotations overlaid from the H&E slides, the mIHC slides were assessed with regard to regions of interest (ROI) located intratumorally (>0.5 mm from the tumor edge), or at the tumor border (within <0.5 mm of the tumor edge) as we have previously described.[14,84] Multiplex staining was performed on 5.0 μm sections and each stained image was scanned at 20x magnification on an Aperio AT2 scanner (Leica Biosystems) prior to image processing.[84] Treg cells were defined as $CD45^+CD3^+CD8^-FOXP3^+$. Human tonsil and spleen were included in all rounds of mIHC as staining controls. Each region was registered to the final hematoxylin using MATLAB Computer Vision Toolbox (The Mathworks, Inc.), color deconvolution and watershed-based nuclei segmentation was performed using ImageJ, and single cell mean intensity for each marker was quantified using Cell Profiler.[85] Single marker positivity thresholds were set using FCS Express Image cytometry RUO (de novo Software) to visually validate marker expression overlaid on signal extracted images.

Statistical Analysis

To calculate z-scores, samples were standardized using the following formula:

$$z = \frac{\textit{experimental value in FPC cohort} - \textit{mean of Control cohort}}{\textit{standard deviation of Control cohort}}$$

This standardization of the data allows for comparison of experimental values across cohorts of FPC-treated mice (including in experiments when the baseline values are significantly different across mouse strains), while preserving the variance of the data by comparing the standard deviations from the mean of the matching Control cohort. Statistical analysis of multiple comparisons was performed using one- or two-way ANOVA with Tukey's HSD post-test, and comparisons between just two groups were performed using a two-tailed Students' unpaired t test with the exception of the patient data, where paired two-tailed t tests were performed. Significance of overall survival was determined via Kaplan-Meier analysis with log-rank analysis and tumor growth kinetics were analyzed with two-way ANOVA with mixed effects modeling. All statistical analyses were performed with Graphpad Prism (GraphPad) for the exact number of mice shown as individual symbols where shown, or as indicated in the legend. Error bars show standard deviation (SD) or standard error of the mean (SEM) shown as indicated in legend, and $p<0.05$ was considered statistically significant. * indicates $p<0.05$, ** $p<0.01$, *** $p< 0.001$, and **** $p< 0.0001$ unless otherwise indicated. *ns* denotes not significant. Significance of cell distribution (distance to edge) was first acquired using the Imaris "shortest distance to edge" calculation. These data were then analyzed using a one-way ANOVA with Tukey's HSD post-test and mean difference analysis to account for the large size of the data sets, and for the graphs, * indicates mean difference of >50 mm, ** >100 mm, *** >150 mm, **** >200 mm in addition to having a p value of <0.001.

Immunity, Volume *59*

Supplemental information

Agonistic anti-CD40 antibody treatment converts resident regulatory T cells into activated type 1 effectors within the tumor microenvironment

Vivien I. Maltez, Charu Arora, Kyle P. Gribbin, Breanna Caruso, Margaret E. Haerr, Rina Sor, Qiaoshi Lian, Katie E. Blise, Shamilene Sivagnanam, Rosalie C. Sears, Lisa M. Coussens, Robert H. Vonderheide, Ronald N. Germain, and Katelyn T. Byrne

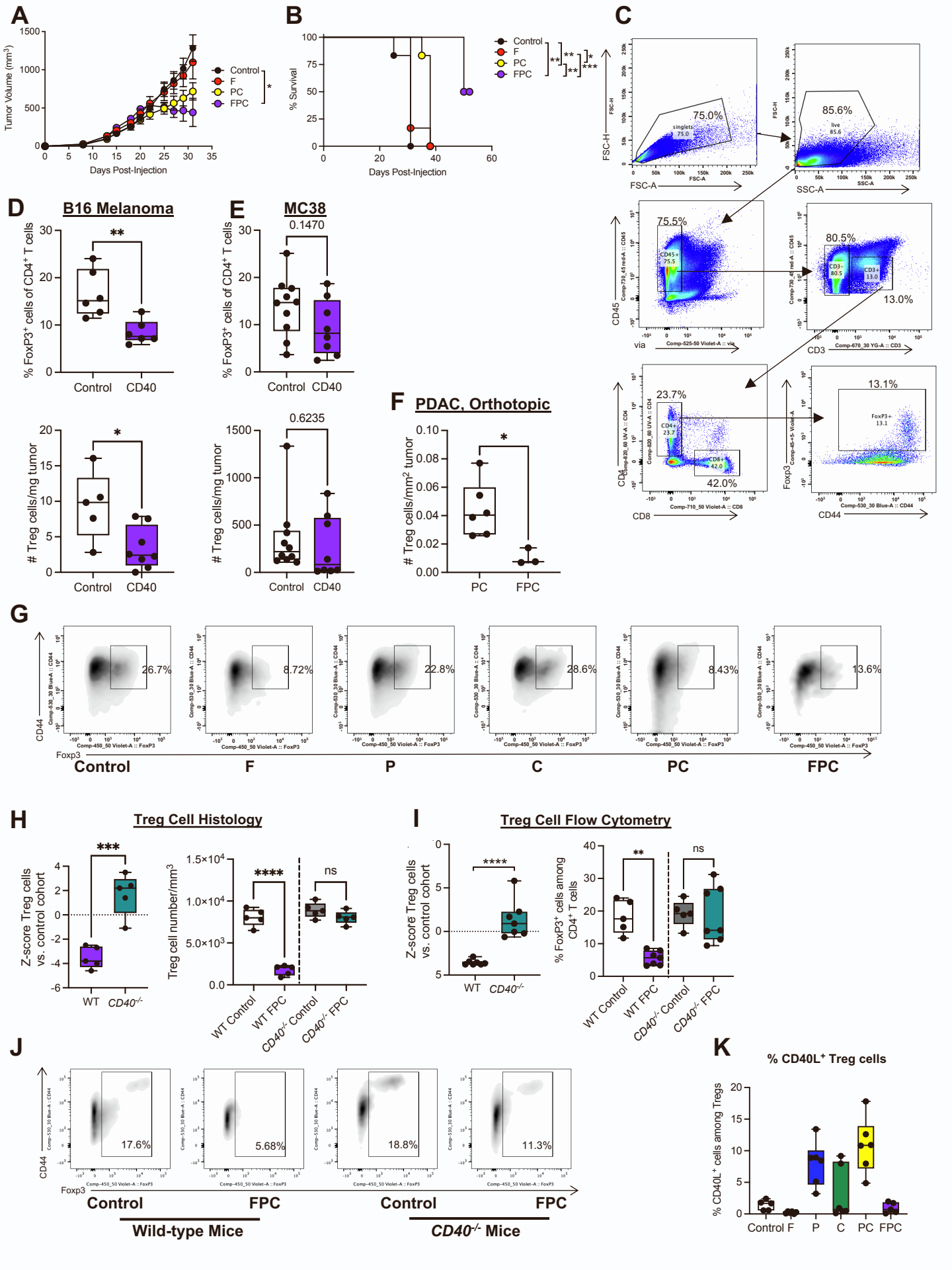
A
Tumor Volume (mm3)
Days Post-Injection
Control
F
PC
FPC
B
% Survival
Days Post-Injection
C
FSC-H
FSC-A
75.0%
singlets
85.6%
live
SSC-A
CD45
CD3
75.5%
80.5%
13.0%
CD4
CD8
23.7%
42.0%
Foxp3
CD44
13.1%
D
B16 Melanoma
% FoxP3+ cells of CD4+ T cells
# Treg cells/mg tumor
Control
CD40
E
MC38
0.1470
0.6235
F
PDAC, Orthotopic
Treg cells/mm2 tumor
PC
FPC
G
26.7%
8.72%
22.8%
28.6%
8.43%
13.6%
CD44
Foxp3
Control
F
P
C
PC
FPC
H
Treg Cell Histology
Z-score Treg cells vs. control cohort
Treg cell number/mm3
WT
CD40-/-
WT Control
WT FPC
CD40-/- Control
CD40-/- FPC
I
Treg Cell Flow Cytometry
% FoxP3+ cells among CD4+ T cells
J
17.6%
5.68%
18.8%
11.3%
Control
FPC
Wild-type Mice
CD40-/- Mice
K
% CD40L+ Treg cells
% CD40L+ cells among Tregs
Control F
P
C
PC
FPC

Supplementary Figure 1. Combination therapy with αCD40 is required for tumor regression and therapeutic efficacy, related to Figure 1. (**A**) Wild-type (WT) C57BL/6 mice were injected with KPCY T cell high tumor clone 2838c3 on day -12 and treated with anti-PD-1 and anti-CTLA-4 (PC) on days 0, 3 and 6, followed by P alone every 3 days, and a single dose of agonistic anti-CD40 (F) on day 3, alone or in combination (FPC) (as described in Figure 1A). Mice were monitored for tumor growth (**A**) and survival (**B**). (**C**) Representative flow gating schema. (**D-E**) $Foxp3^+$ cells among live, $CD4^+CD3^+CD45^+$ cells were quantified by flow cytometry with regard to proportion (top) or absolute count per mg of tumor (bottom) in B16 melanoma (**D**), or MC38 (**E**). (**F**) KPCY T cell high tumor clone 2838c3 was orthotopically implanted 18 days prior to the start of treatment as in Figure 1A, tumors were harvested 48 hours after FPC and tissue sections were stained for $Foxp3^+CD3^+$ cells. (**G**) Representative flow plots of data from Figure 1F, gated on live, $CD45^+CD3^+CD4^+$ cells. (**H-J**) $CD40^{-/-}$ mice were treated as described in Figure 1A along with concurrent wildtype (WT) mice, and analyzed with regard to $Foxp3^+$ cells among live, $CD4^+CD3^+CD45^+$ cells via histology (**H**) and flow cytometry (**I**), with representative flow plots shown in (**J**). Standardized to Treg cell proportions in the control treated cohort within each genotype in left side graphs of (**H, I**). (**K**) CD40 ligand expression within Treg cells after the indicated treatments. Data representative of n=2 independent experiments with n=3-10 mice per group. Analysis by two-way ANOVA (**A**), Mantel-Cox log-rank analysis (**B**), or unpaired T test (**D-F, H, I**). In (**H, I**), data were standardized and compared by one-way ANOVA for left side graphs. * indicates $p<0.05$, ** indicates $p<0.01$, *** indicates $p<0.001$, ns denotes not significant.

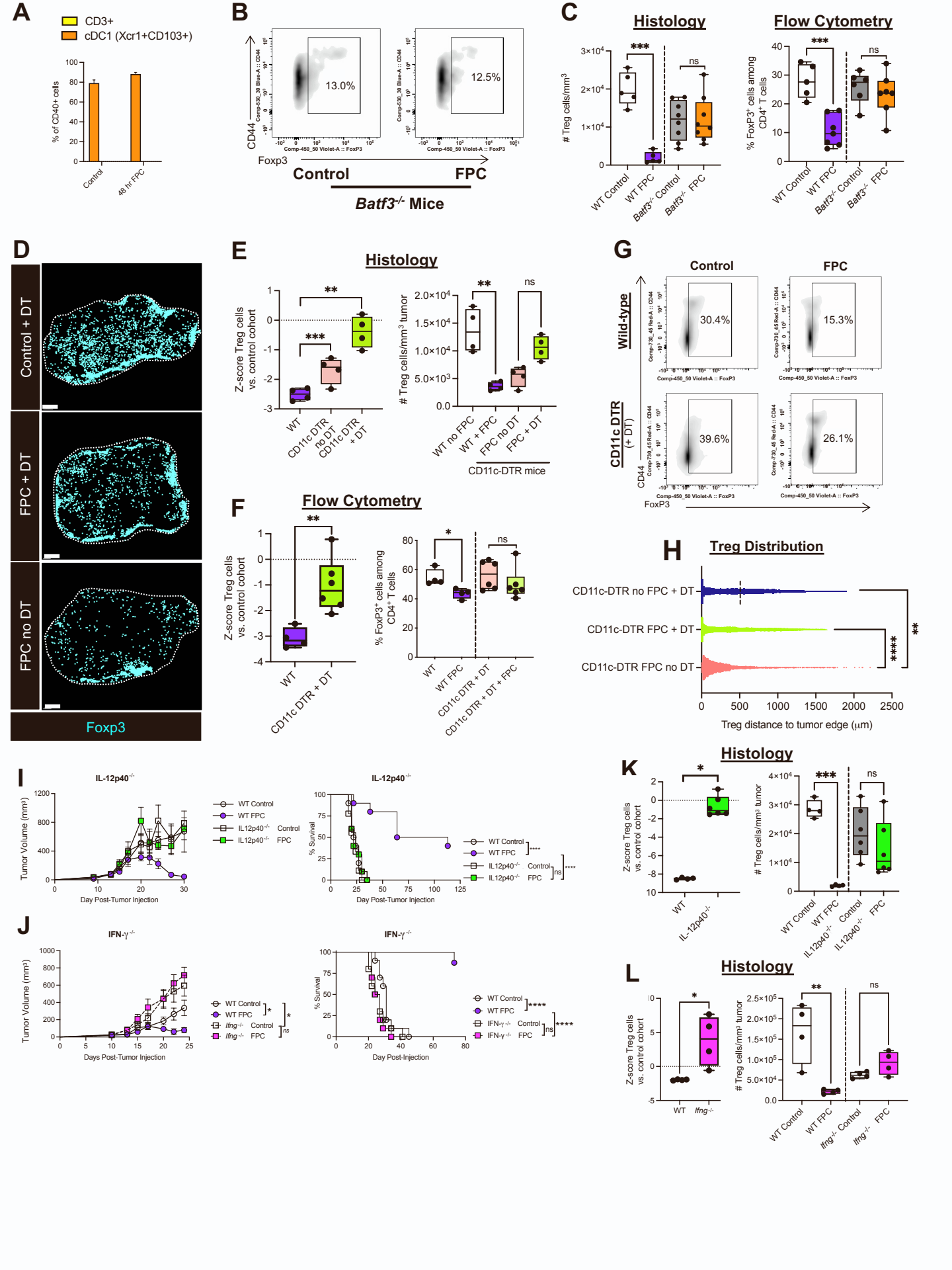
A
CD3+
cDC1 (Xcr1+CD103+)
% of CD40+ cells
Control
48 hr FPC
B
13.0%
12.5%
CD44
Foxp3
Control
FPC
Batf3-/- Mice
C
Histology
Treg cells/mm3
***
ns
WT Control
WT FPC
Batf3-/- Control
Batf3-/- FPC
Flow Cytometry
% FoxP3+ cells among CD4+ T cells
D
Control + DT
FPC + DT
FPC no DT
Foxp3
E
Histology
Z-score Treg cells vs. control cohort
Treg cells/mm3 tumor
WT
CD11c DTR no DT
CD11c DTR + DT
WT no FPC
WT + FPC
FPC no DT
FPC + DT
CD11c-DTR mice
F
Flow Cytometry
Z-score Treg cells vs. control cohort
% FoxP3+ cells among CD4+ T cells
WT
WT FPC
CD11c DTR + DT
CD11c DTR + DT + FPC
G
Control
FPC
Wild-type
CD11c DTR (+ DT)
30.4%
15.3%
39.6%
26.1%
CD44
FoxP3
H
Treg Distribution
CD11c-DTR no FPC + DT
CD11c-DTR FPC + DT
CD11c-DTR FPC no DT
Treg distance to tumor edge (μm)
I
IL-12p40-/-
Tumor Volume (mm3)
Day Post-Tumor Injection
WT Control
WT FPC
IL12p40-/- Control
IL12p40-/- FPC
% Survival
J
IFN-γ-/-
Tumor Volume (mm3)
Days Post-Tumor Injection
Ifng-/- Control
Ifng-/- FPC
IFN-γ-/- Control
IFN-γ-/- FPC
Day Post-Injection
K
Histology
Z-score Treg cells vs. control cohort
Treg cells/mm3 tumor
WT
IL-12p40-/-
L
Histology
Z-score Treg cells vs. control cohort
Treg cells/mm3 tumor
Ifng-/-

Supplementary Figure 2. Dendritic cells and the IFN-γ/IL-12 axis mediate αCD40-induced reduction of intratumoral Treg cells, related to Figure 2. (**A**) Quantification of CD40 expression via RNAscope of whole tumors among *Cd3*$^{+}$ cells (yellow) or cDC1s (defined as *Cd3*$^{-}$*Xcr1*$^{+}$*Cd103*$^{+}$ cells) in Foxp3-Lineage mice treated as in Figure 3. (**B**-**C**) *Batf3*$^{-/-}$ mice were treated as described in Figure 1A for WT-mice, and the proportion of Foxp3^{+} cells among live, CD45^{+}CD3^{+}CD4^{+} cells (**B**) was quantified (**C**). (**D-H**) CD11c DTR mice were treated as described in Figure 1A except indicated groups also received DT 24 hours before and after CD40 administration prior to assessment for Treg cell abundance (**D**), quantified by histology (**E**) or flow cytometry (**F**) with representative flow plots shown in (**G**), gated on live, CD45^{+}CD3^{+}CD4^{+} cells, and distribution of Treg cells in the tumor site shown in (**H**). (**I-L**) Experiments were performed in tumor-bearing wild-type, IL-12p40$^{-/-}$ or IFN-γ$^{-/-}$ mice, as indicated. (**I-J**) Tumor-growth kinetics (right) or survival curves (left) from IL-12p40$^{-/-}$ (**I**) and IFN-γ$^{-/-}$ mice (**J**). (**K-L**) Histological analysis of IL-12p40$^{-/-}$ and IFN-γ$^{-/-}$ mice with standardized z-scores compared to Control cohort (left) with raw numbers (right). Data are representative of 2-3 independent experiments with n=3-12 mice per group, each symbol represents an individual mouse (**C, E, F, K, L**), an individual cell (**H**), or the mean of the group as indicated (**A, I, J**), error bars indicate SEM (A, **I, J**) or SD (**C, E, F, K, L**), horizontal line indicates median (**C, E, F, K, L**). For analysis, (**A** and **H**) had 3 mice/group. Scale bars are 300 μm (**D**), and the dotted line indicates tumor edge. Analysis by unpaired T-test (**C, F, K, L**), between indicated groups for raw data left or bottom, or z-scored standardized data, one-way ANOVA (**E**) with Tukey's post-test, one-way ANOVA with Tukey's post-test and mean difference calculations to account for effect size (**H**), two-way ANOVA with mixed effect modeling with Tukey's post-hoc

analysis (**I, J**, left panels), or Mantel-Cox log-rank analysis (**I, J**, right panels). * indicates $p<0.05$, ** indicates $p<0.01$, **** indicates $p<0.0001$, *ns* indicates not significant. For the distance to edge plot (**H**): ANOVA p value summary is <0.0001, with symbols indicating statistically significant mean difference of * for >50 μm, ** for >100 μm, *** for >150 um, **** for >200 μm, or *ns* for not significant.

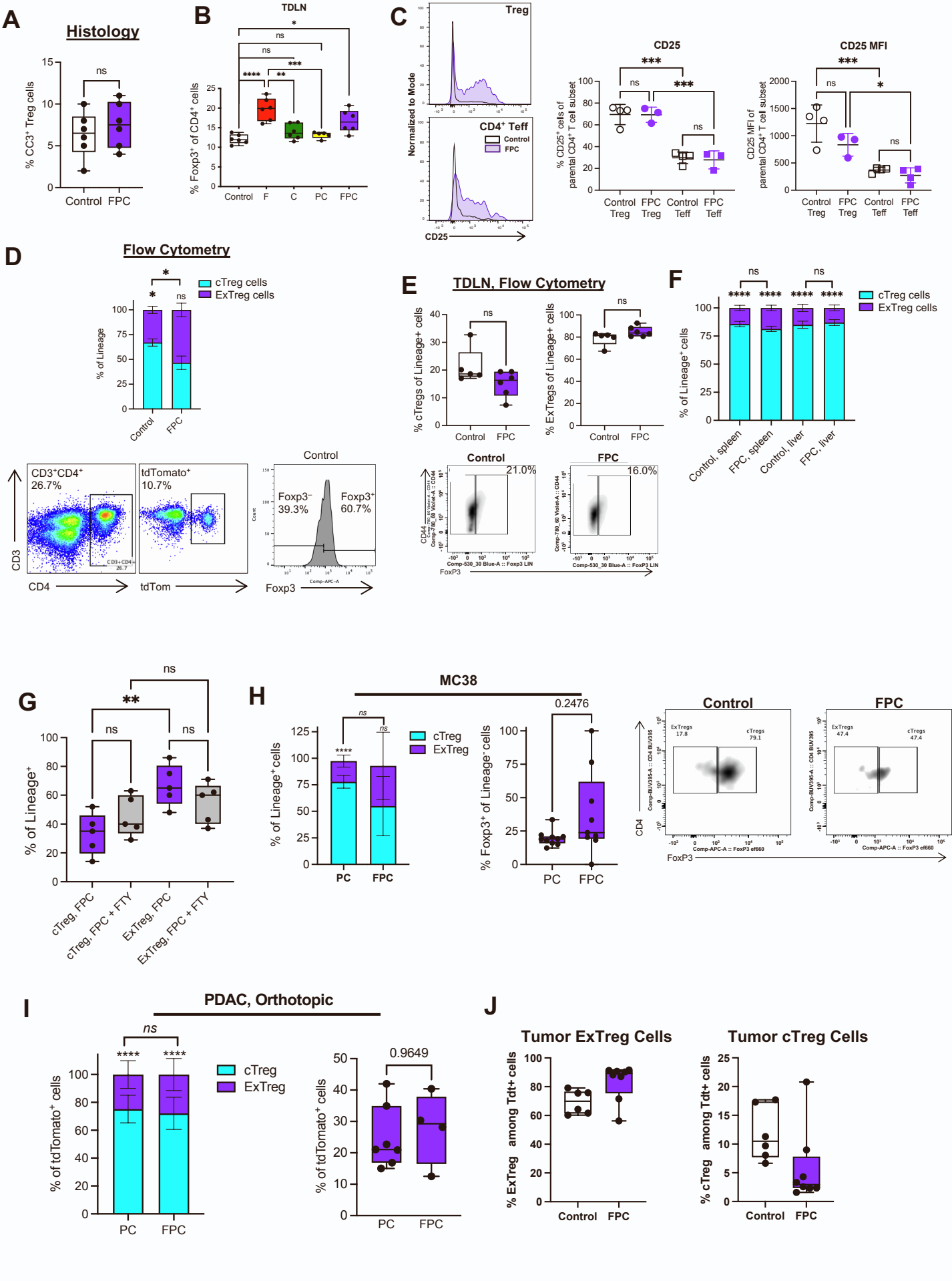
A
Histology
% CC3+ Treg cells
ns
Control FPC
B
TDLN
% Foxp3+ of CD4+ cells
Control F C PC FPC
C
Treg
Normalized to Mode
CD4+ Teff
Control
FPC
CD25
CD25
% CD25+ cells of parental CD4+ T cell subset
Control Treg FPC Treg Control Teff FPC Teff
CD25 MFI
CD25 MFI of parental CD4+ T cell subset
D
Flow Cytometry
cTreg cells
ExTreg cells
% of Lineage
Control FPC
CD3+CD4+ 26.7%
tdTomato+ 10.7%
CD3
CD4
tdTom
Control
Foxp3− 39.3%
Foxp3+ 60.7%
Foxp3
E
TDLN, Flow Cytometry
% cTregs of Lineage+ cells
% ExTregs of Lineage+ cells
Control FPC
Control
FPC
21.0%
16.0%
CD44
FoxP3
F
% of Lineage+ cells
cTreg cells
ExTreg cells
Control, spleen
FPC, spleen
Control, liver
FPC, liver
G
% of Lineage+
cTreg, FPC
cTreg, FPC + FTY
ExTreg, FPC
ExTreg, FPC + FTY
H
MC38
% of Lineage+ cells
cTreg
ExTreg
PC FPC
% Foxp3+ of Lineage- cells
0.2476
Control
FPC
CD4
FoxP3
ExTregs 17.8
cTregs 79.1
ExTregs 47.4
cTregs 47.4
I
PDAC, Orthotopic
% of tdTomato+ cells
cTreg
ExTreg
PC FPC
0.9649
J
Tumor ExTreg Cells
% ExTreg among Tdt+ cells
Control FPC
Tumor cTreg Cells
% cTreg among Tdt+ cells
Control FPC

Supplementary Figure 3. CD40 agonism promotes the ExTreg cell state among $CD4^+$ T cells within the TME, related to Figure 3.

(**A-C**) Wild-type mice were treated as described in Figure 1A. (**A**) Treg cellular expression of cleaved caspase 3 (CC3) +/- FPC treatment in wild-type mice via histological analysis. (**B**) Proportions of $FoxP3^+CD4^+$ Treg cells among live, $CD45^+CD3^+$ cells in the tumor draining lymph node (TDLN) as assessed by flow cytometry. (**C**) WT mice were treated as in Figure 1A and tumors were analyzed by flow cytometry for CD25 among Treg or effector T (T_{eff}) cells defined as live, $CD45^+CD3^+CD4^+FoxP3^-$ cells, with a representative histogram shown on the left from mice treated with vehicle Control (open) or FPC (purple). (**D-J**) FoxP3-Lineage mice were treated as described in Figure 3. (**D**) Proportion of cTreg ($CD3^+CD4^+tdTomato^+Foxp3^+$, cyan) or ExTreg ($CD3^+CD4^+tdTomato^+Foxp3^-$, purple) cells among tdTomato+ Lineage marked cells (3 mice for Control and 4 for FPC). Representative flow plot shown below. (**E**) cTreg ($tdTomato^+Foxp3^+$) or ExTreg ($tdTomato^+Foxp3^-$) cells among live, $CD45^+CD3^+CD4^+$ T cells in the TDLN of Foxp3-Lineage mice, representative flow plots shown below. (**F**) Proportion of cTreg vs. ExTreg cells in control vs. FPC treated mice in the spleen and liver of Foxp3-Lineage mice as assessed by histological analysis as in (**D**). (**G**) Foxp3-Lineage mice were treated +/- FTY720 daily at the start of FPC treatment and proportions of intratumoral cTreg or ExTreg cell populations were analyzed at 48 hrs. (**H**) cTreg ($tdTomato^+Foxp3^+$) or ExTreg ($tdTomato^+Foxp3^-$) cells among live, $CD45^+CD3^+CD4^+$ T cells in MC38 tumors from Foxp3-Lineage mice, representative flow plots shown below. (**I**) Foxp3-Lineage mice received ultrasound guided orthotopic tumor injection on day 0, followed by TMX on days 6-8, PC on days 9 and 12, with F on day 12 as indicated (FPC), or Isotype Controls,

followed by takedown on day 14. Analyzed by IF for proportions of FoxP3$^+$ cells among tdTomato$^+$ cells. (**J**) Day 10 post anti-CD40 cTreg and ExTreg cell proportions within the tumor. Data are representative of 2-5 independent experiments with n=3-12 mice per group; each symbol represents an individual mouse, horizontal lines indicate the median, bars show interquartile range, and whiskers indicate the range, and error bars indicate SD (**A-E, G**, **H** right, **I** right), or the colors indicate the relative proportion of cTreg or ExTreg cells and the error bars indicate the SD (**F, H** left, **I** left, n of mice/group shown on right for **H** & **I**). For analysis, panel (**D**) had 3 control and 4 FPC-treated, (**F**) had 3 mice/group, Analysis by unpaired T-test (**A, D, E, H** right**, I** right, **J**), one-way ANOVA with Tukey's post-test (**B, C, G**), or two-way ANOVA with Tukey's post-test (**F, H** left**, I** left). For p values, * indicates $p<0.05$, ** indicates $p<0.01$, *** indicates $p<0.001$, **** indicates $p<0.0001$, *ns* indicates not significant.

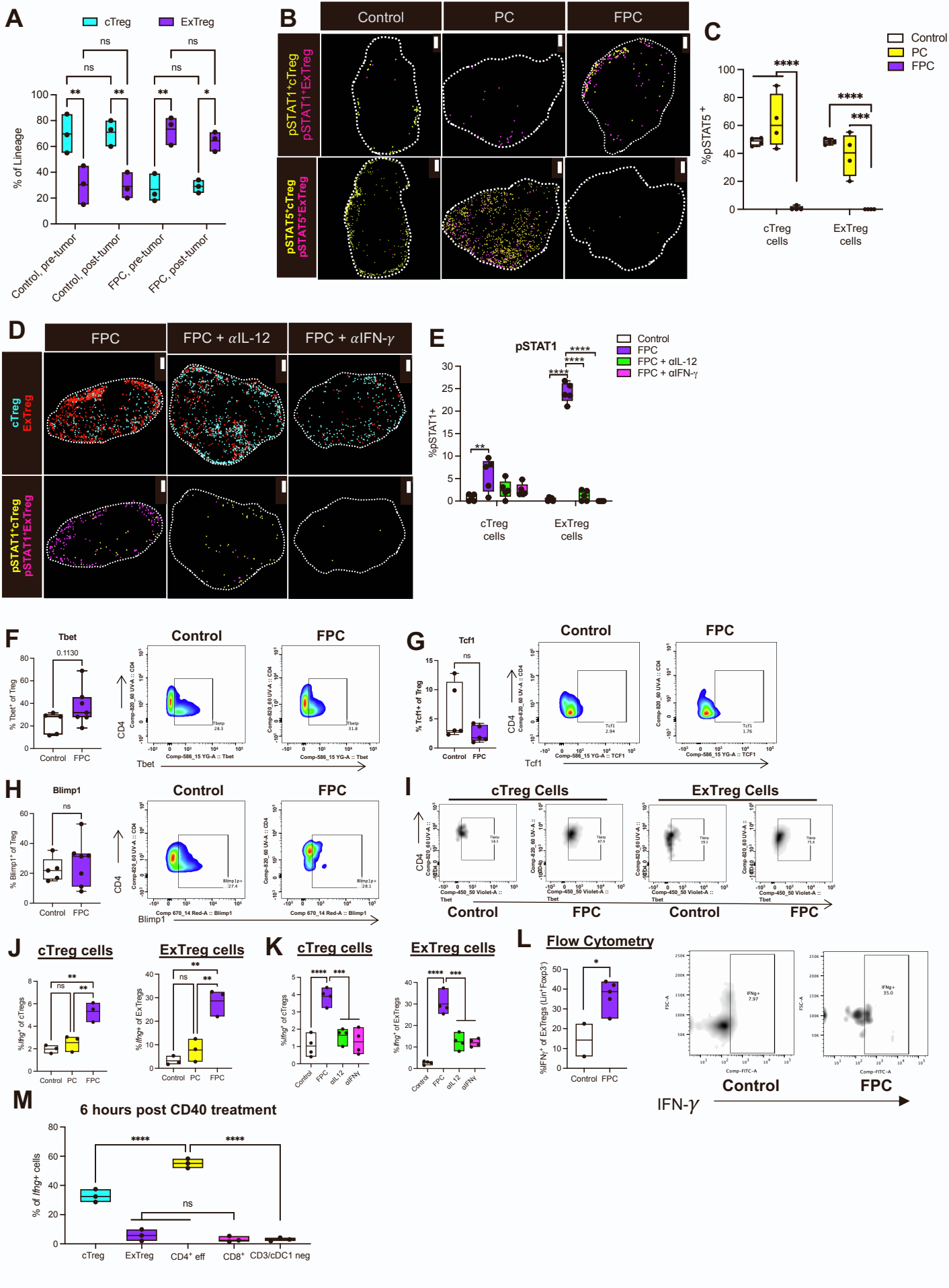
A
cTreg
ExTreg
% of Lineage
Control, pre-tumor
Control, post-tumor
FPC, pre-tumor
FPC, post-tumor
B
Control
PC
FPC
pSTAT1+cTreg
pSTAT1+ExTreg
pSTAT5+cTreg
pSTAT5+ExTreg
C
Control
PC
FPC
%pSTAT5+
cTreg cells
ExTreg cells
D
FPC
FPC + αIL-12
FPC + αIFN-γ
cTreg
ExTreg
pSTAT1+cTreg
pSTAT1+ExTreg
E
pSTAT1
Control
FPC
FPC + αIL-12
FPC + αIFN-γ
%pSTAT1+
cTreg cells
ExTreg cells
F
Tbet
0.1130
% Tbet+ of Treg
Control
FPC
CD4
Tbet
G
Tcf1
ns
% Tcf1+ of Treg
Control
FPC
CD4
Tcf1
H
Blimp1
ns
% Blimp1+ of Treg
Control
FPC
CD4
Blimp1
I
cTreg Cells
ExTreg Cells
CD4
Tbet
Control
FPC
Control
FPC
J
cTreg cells
ExTreg cells
%Ifng+ of cTregs
%Ifng+ of ExTregs
Control
PC
FPC
K
cTreg cells
ExTreg cells
%Ifng+ of cTregs
%Ifng+ of ExTregs
Control
FPC
αIL12
αIFNγ
L
Flow Cytometry
%IFNγ+ of ExTregs (Lin+Foxp3+)
Control
FPC
IFNg+
7.97
IFNg+
35.0
FSC-A
Comp-FITC-A
Control
FPC
IFN-γ
M
6 hours post CD40 treatment
% of Ifng+ cells
cTreg
ExTreg
CD4+ eff
CD8+
CD3/cDC1 neg

Supplementary Figure 4. Transcriptional skewing after CD40 agonism, related to Figure 4. (**A**) Foxp3-Lineage mice either received tamoxifen as described in **Figure 3** (8-10 days post-tumor) or 2 weeks prior to tumor injection (pre-tumor) followed by treatment as described in Figure 1A for cell number, viability, and location of tumor implantation and following immunotherapy. Tumors were then analyzed for the proportions of cTreg and ExTreg cells in vehicle control vs. FPC-treated mice. (**B-D**) Foxp3-Lineage mice were treated as described in Figure 3. (**B-C**) Representative pSTAT1 (top) and pSTAT5 (bottom) staining by the indicated Lineage subsets in tumors from Foxp3-Lineage mice with vehicle control, PC, or FPC, quantified in main Figure 4C and (**C**). (**D-E**) Representative pSTAT1 staining by the indicated Lineage subsets in tumors from Foxp3-Lineage mice after treatment with FPC or FPC with blockade against IL-12p40 or IFN-γ, quantified in (**E**). (**F-H**) WT mice were treated as in Figure 1A and tumors were analyzed by intracellular flow cytometry for indicated transcription factor expression among live, protein-stained, $CD45^+CD3^+CD4^+Foxp3^+$ T cells as indicated, quantified on the left, with a representative flow plot shown on the right for Tbet (**F**), Tcf1 (**G**), and Blimp (**H**) from mice treated with vehicle Control (open) or FPC (purple). (**I**) Representative flow plots for Tbet expression shown in Figure 4F from Foxp3-Lineage mice treated described in Figure 3. (**J-M**) Foxp3-Lineage mice were treated as described in Figure 4. (**J**) Quantification of *Ifng*$^+$ cTreg and ExTreg cells after treatment with vehicle control, PC, or FPC. (**K**) Quantification of *Ifng*$^+$ cTreg and ExTreg cells after treatment with vehicle control, FPC, or FPC and IL-12p40 or IFN-γ blocking antibody. (**L**) Quantification of IFN-γ protein-expressing cells by intracellular cytokine staining via flow cytometry in Control and FPC treated mice among live $CD45^+CD3^+CD4^+Lineage^+Foxp3^-$ cells, representative flow plots

shown to the right. (**M**) Histological quantification of the proportion of *Ifng*$^{+}$ cells among indicated parental cell population at 6 hours after αCD40. Data representative of 2-5 independent experiments with n=3-12 mice per group, with the exception of **A**, which was performed once with 3 mice per group. Scale bars are 300 μm and the dotted line indicates tumor edge. Each symbol represents an individual mouse, (**A, J-M**) horizontal lines indicate the mean, boxes indicate range, (**C, E, F, H**) horizontal lines indicate the median and whiskers indicate range. Analysis by two-way ANOVA with Tukey's post-test (**A, I**), one-way ANOVA with Tukey's post-test (**C, E, J, K, M**) or unpaired T-test (**F, G, H, L**). For p values, * indicates $p<0.05$, ** $p<0.01$, *** $p<0.001$, **** $p<0.0001$, *ns* indicates not significant.

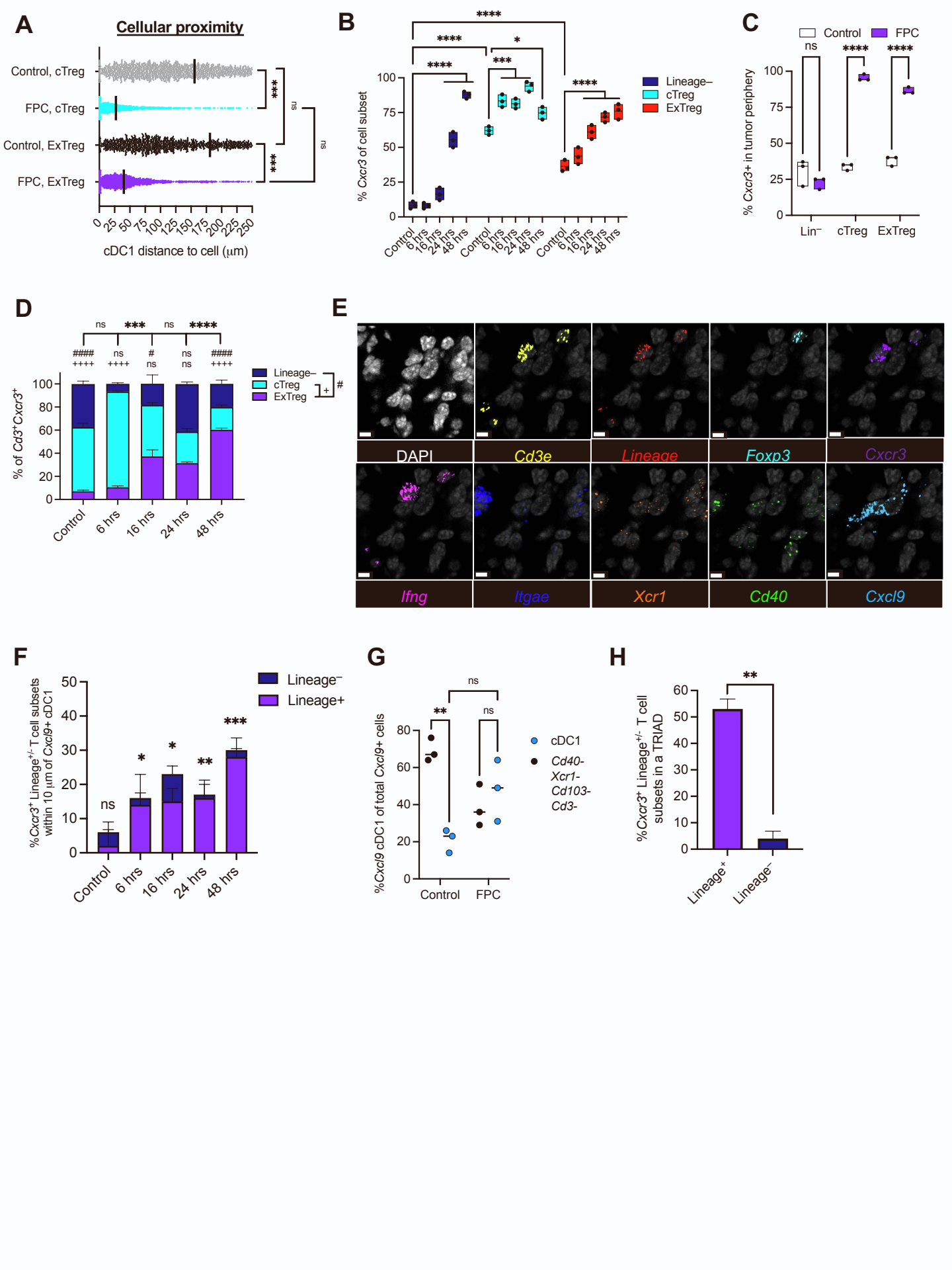
A
Cellular proximity
Control, cTreg
FPC, cTreg
Control, ExTreg
FPC, ExTreg
***
ns
***
ns
0 25 50 75 100 125 150 175 200 225 250
cDC1 distance to cell (μm)
B
% Cxcr3 of cell subset
Lineage–
cTreg
ExTreg
Control 6 hrs 16 hrs 24 hrs 48 hrs
C
Control
FPC
% Cxcr3+ in tumor periphery
Lin–
cTreg
ExTreg
D
% of Cd3+Cxcr3+
Lineage–
cTreg
ExTreg
Control
6 hrs
16 hrs
24 hrs
48 hrs
E
DAPI
Cd3e
Lineage
Foxp3
Cxcr3
Ifng
Itgae
Xcr1
Cd40
Cxcl9
F
%Cxcr3+ Lineage+/- T cell subsets within 10 μm of Cxcl9+ cDC1
Lineage–
Lineage+
G
%Cxcl9 cDC1 of total Cxcl9+ cells
Control
FPC
cDC1
Cd40-
Xcr1-
Cd103-
Cd3-
H
%Cxcr3+ Lineage+/- T cell subsets in a TRIAD
Lineage+
Lineage–

Supplementary Figure 5. *Cxcr3* and *Cxcl9* expression increase in the tumor periphery after CD40 agonism, related to Figure 5. Tamoxifen-inducible (TMX) Foxp3-Lineage tracing mice (treated as in Figure 3) and RNAscope technology were used for all experiments described. (**A**) Quantification of the proximity of the indicated T cell subsets to cDC1s at 48 hours after FPC treatment. (**B**) Mice were treated as described in Figure 5A and analyzed for *Cxcr3* expression via RNAscope. Proportions of *Cxcr3*$^{+}$ cells within the indicated subset (**B**) and in the tumor periphery (**C**), defined as the region within 250 μm of the tumor border (as described in Figure 5). (**D**) Stacked bar graph indicating the T cell subset breakdown of *Cd3*$^{+}$ *Cxcr3*$^{+}$ cells. (**E**) Single RNA probe marker images for the merge images in Figure 5K. (**F**) Proportion of *Cxcr3*$^{+}$ cells that are within 10 μm of *both* a *Cxcl9*$^{+}$ non-cDC1 *and* a *Cxcl9*$^{–}$ cDC1. (**G**) Proportion of *Cxcl9*$^{+}$ cells that are cDC1s in vehicle control vs. FPC treated mice. (**H**) Proportion of *Cxcr3*$^{+}$ cells that are within 10 μm of *both* a *Cxcl9*$^{+}$ non-cDC1 *and* a *Cxcl9*$^{–}$ cDC1. Data representative of 2 independent experiments with n=3-4 mice per group; each symbol represents an individual mouse (**B, C, G**) or individual cell (**A**), horizontal lines indicate the median, error bars indicate SEM (**D**) or SD (**F, H**). For analysis, panels (**A**), (**D**), (**F**, **H**) had 3 mice/group. Scale bars are 5 μm (**E**). Analysis by one-way ANOVA with Tukey's post-test and mean difference calculation to adjust for effect size (**A**), one-way ANOVA with Tukey's post-test (**A**), two-way ANOVA with Tukey's post-test (**B, C, D, F, H**), or unpaired T-test (**G**). For p values, * indicates $p<0.05$, ** $p<0.01$, *** $p<0.001$, **** $p<0.0001$, *ns* indicates not significant. (**D**) Comparisons between navy (*Lineage*$^{-}$) and purple (ExTreg cells) are represented with a (#), between navy (*Lineage*-) and cyan (cTreg cells) with a (+), and between purple over time with a (*). All symbols use the same scaling as described for p values with (*).

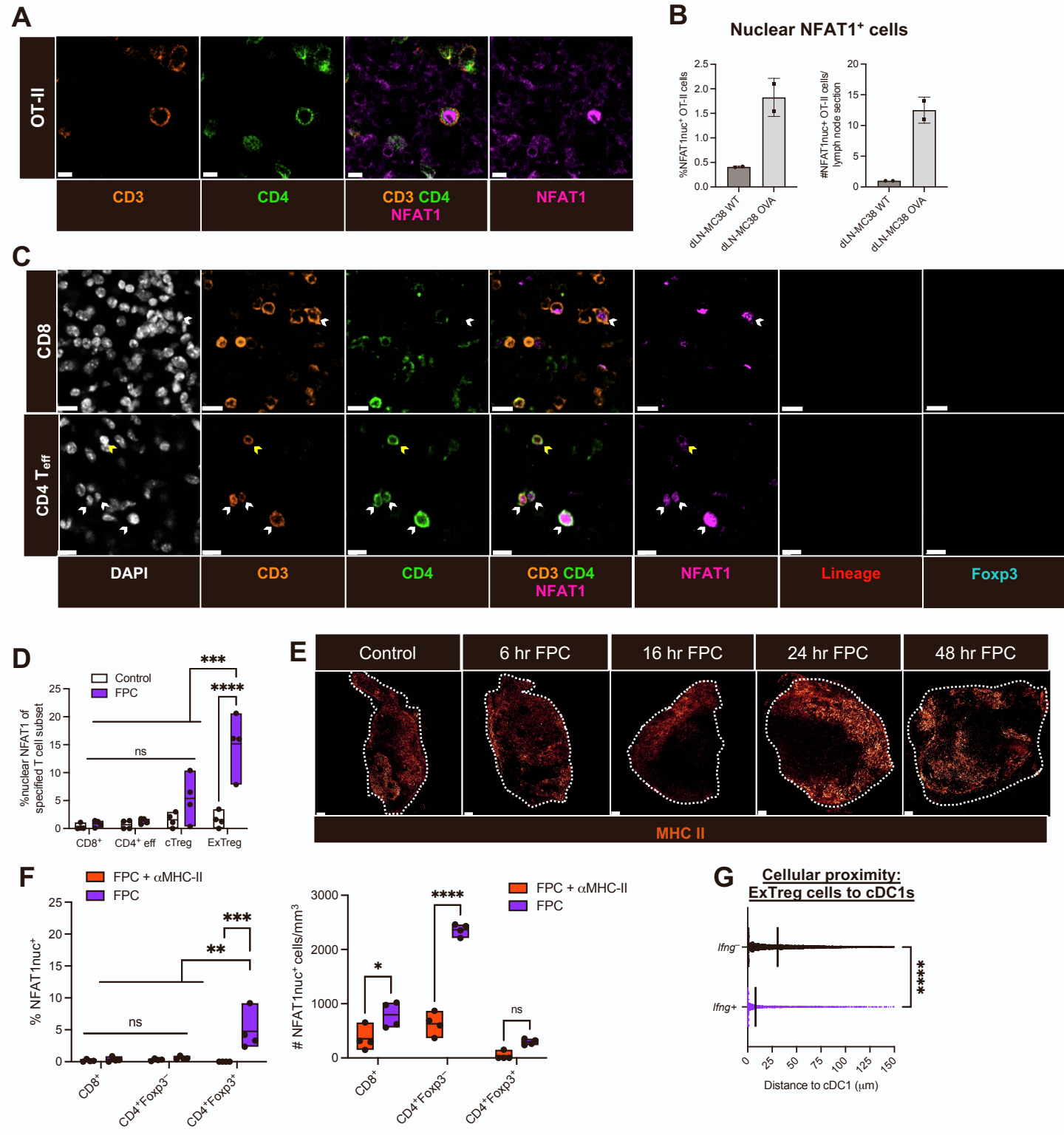
A
OT-II
CD3
CD4
CD3 CD4 NFAT1
NFAT1
B
Nuclear NFAT1+ cells
%NFAT1nuc+ OT-II cells
#NFAT1nuc+ OT-II cells/ lymph node section
dLN-MC38 WT
dLN-MC38 OVA
C
CD8
CD4 Teff
DAPI
CD3
CD4
CD3 CD4 NFAT1
NFAT1
Lineage
Foxp3
D
Control
FPC
%nuclear NFAT1 of specified T cell subset
ns
CD8+
CD4+ eff
cTreg
ExTreg
E
Control
6 hr FPC
16 hr FPC
24 hr FPC
48 hr FPC
MHC II
F
FPC + αMHC-II
FPC
% NFAT1nuc+
# NFAT1nuc+ cells/mm3
CD8+
CD4+Foxp3-
CD4+Foxp3+
G
Cellular proximity: ExTreg cells to cDC1s
Ifng-
Ifng+
Distance to cDC1 (μm)

Supplementary Figure 6. NFAT1 translocation is detectable in T cell subsets in situ, related to Figure 6.

(**A-B**) MC38-OVA or MC38-WT bearing *Rag1* mice were adoptively transferred with $1x10^6$ in vitro activated OT-II cells. The tumor draining lymph node was analyzed for NFAT1nuc signal in OT-II cells (**A**) by percentage (**B**, left) and average number per section for the entire tissue (**B**, right). (**C-D**) Foxp3-lineage mice were treated as described in Figure 3. (**C**) Representative tumor immunostaining for NFAT1nuc (white arrows) and membrane NFAT1 (yellow arrows) expression within $CD8^+$ (**C**, upper), and effector $CD4^+$ (non-Treg) (**C**, lower) conventional (T_{conv}) T cells in tumor-bearing Foxp3-Lineage mice 48 hours after FPC treatment. (**D**) Percentage of T cell subsets with nuclear NFAT1 localization 48 hours post-CD40 treatment. (**E-F**) WT mice were treated as in Figure 1A and received anti-MHC II blockade as in Figure 6J, with representative MHC II staining over time post-CD40 administration. (**F**) WT mice were treated as in Figure 1A +/- MHC II blockade and NFAT1nuc staining in the tumor site was quantified by absolute count (**F**, left) and proportion (**F**, right) among indicated cell populations. (**G**) Foxp3-Lineage mice were treated as in Figure 3. The proximity of cDC1 (defined as: *Cd3*$^-$*Itgae*$^+$*Xcr1*$^+$) proximity to *Ifng*$^-$ or *Ifng*$^+$ ExTreg cells within 3 FPC-treated mice (for analysis). Data representative of 1-3 independent experiments with n=2-4 mice per group; each symbol represents an individual mouse; horizontal lines indicate the median. Scale bars are 5 μm (**A, C**) or 300 μm (**E**). Analysis by unpaired T-test (**G**) or two-way ANOVA with Tukey's post-test (**D, F**). For p values, * indicates $p<0.05$, ** $p<0.01$, *** $p<0.001$, **** $p<0.0001$, *ns* indicates not significant.